Computational Analyses of Offset Stream Nozzles for Noise Reduction

Vance Dippold, III*, Lancert Foster
NASA Glenn Research Center, Cleveland, OH 44135

and

Michael Wiese
Analytical Services and Materials, Hampton, VA 23681

The Wind computational fluid dynamics code was used to perform a series of simulations on two offset stream nozzle concepts for jet noise reduction. The first concept used an S-duct to direct the secondary stream to the lower side of the nozzle. The second concept used vanes to turn the secondary flow downward. The analyses were completed in preparation of tests conducted in the NASA Glenn Research Center Aeroacoustic Propulsion Laboratory. The offset stream nozzles demonstrated good performance and reduced the amount of turbulence on the lower side of the jet plume. The computer analyses proved instrumental in guiding the development of the final test configurations and giving insight into the flow mechanics of offset stream nozzles. The computational predictions were compared with flowfield results from the jet rig testing and showed excellent agreement.

Nomenclature

AOA	=	vane angle of attack
Cd	=	discharge coefficient
Cfg	=	thrust coefficient
D	=	diameter of secondary flow nozzle exit
$F_{momentum}$	=	integrated momentum force on nozzle
$F_{pressure}$	=	integrated pressure force on nozzle
$F_{viscous}$	=	integrated viscous force on nozzle
k	=	turbulent kinetic energy
k^*	=	non-dimensionalized value of turbulent kinetic energy; $k^* = \frac{k}{u_{jet}^2}$
$(k^*)_{peak}$	=	maximum value of k^* in upper of lower region of plume
M	=	local Mach number
M_∞	=	freestream Mach number
$\dot{m}$	=	mass flow rate
p_∞	=	freestream static pressure
p_0/p_∞	=	nozzle pressure ratio
T_∞	=	freestream static temperature
T_0	=	nozzle plenum total temperature
u	=	local axial velocity
u_{jet}	=	mass-averaged axial velocity of primary jet
x, y, z	=	coordinate system
$\Delta(\ )$	=	used to denote difference in discharge or thrust coefficient of the current configuration from the baseline configuration

I. Introduction

Today's jetliners are significantly more efficient and quieter when compared to commercial jetliners of the 1960s and 1970s. Even so, the goal of reducing noise from aircraft in communities surrounding airports continues to exist. Aircraft manufacturers are motivated more and more by stringent noise abatement regulations in airport communities. Traditionally, much of the noise heard

* Member AIAA

during take-off and landing comes from the aircraft's engines, and much of that noise is jet noise. Jet noise is produced by the shear layers of the jet plume: the core stream, fan stream, and freestream.

Much research has been exerted on jet engine nozzles to hasten the mixing of the shear layers without significantly reducing performance. In the past, this was accomplished using lobed mixer nozzles. More recently, the addition of chevrons[1-9] has been examined and found to reduce noise by up to 2.5 EPNdB during installed testing. However, while nozzles with chevrons can significantly reduce low frequency noise, they do so at the expense of increasing high frequency noise.

Papamoschou investigated offsetting the fan stream using vanes and wedges[10-13]. The idea was to direct the fan stream to the lower side of the jet plume and to shield the observer on the ground from jet noise. Papamoschou reported very positive results from his offset fan stream experiments. Zaman also investigated offset fan stream nozzles with his eccentric nozzle and found favorable noise reduction[14].

NASA's Offset Stream Technologies task aimed to expand these earlier works. Flowfield and acoustical measurements were taken of offset stream nozzles using vanes, S-ducts, and wedges to achieve the offset fan stream. Higher bypass ratio nozzles were used, as that is the direction the industry is headed. Additionally, the tests used larger scale models and heated core primary flows. The work presented in this discussion involves the Computational Fluid Dynamic (CFD) analyses performed on S-duct and vane offset stream nozzles in preparation for the jet rig testing.

II. Present Goals

The primary purpose for this set of CFD analyses for offset stream nozzle configurations was to prepare for experimental testing in the Aeroacoustic Propulsion Lab (AAPL) at NASA's Glenn Research Center. Before manufacturing hardware, it was necessary to verify that the nozzle configurations produced jet flows as expected: jet flows free from significant loses and noise sources, such as shocks or flow separations. An aim of the computational analyses was to also help determine what configuration parameters were important (such as vane angle of attack and axial and azimuth locations) and what hardware should be manufactured. Additionally, the CFD solutions predicted what types of loads the vanes would see, so that they could be manufactured to withstand such loads. The CFD solutions also allowed the observation of parts of the flow that could not be easily observed during the AAPL testing, such as the internal flow around the vanes. Finally, the CFD solutions could be coupled with the JeNo computational aeroacoustics code[15] to obtain noise prediction results for validation.

III. Modeling

A. Nozzle Configurations

Two dual-stream subsonic nozzle models were used for this computational study: the 5BB nozzle from Glenn Research Center; and a nozzle from Langley Research Center. Both nozzles were developed to study nozzle flows with a bypass ratio of eight. These flowlines for the baseline nozzles are illustrated in Figure 1. The 5BB nozzle had a fan stream nozzle diameter D of 9.63 inches, and the LaRC nozzle had a fan stream nozzle diameter D of 9.42 inches.

Three S-duct configurations were tested. The fan stream was offset from the axis using an S-duct located upstream of where the fan stream nozzle converged. Previous studies found poor performance when incorporating the S-duct into the convergent portion of the fan stream nozzle. Two S-duct configurations used the LaRC baseline nozzle, with offsets of 9.3% D and 4.6% D; and one S-duct configuration was based on the 5BB baseline, with an offset of 4.5% D. These configuration parameters are listed in Table 1 for each S-duct nozzle. Figure 2 shows the flowlines of the three S-duct configurations, and Figure 3 shows a rendering of the Sduct-5BB-45 nozzle.

Table 1: S-duct nozzle configurations

Configuration	Baseline	S-duct Offset
Sduct-LaRC-93	LaRC BPR8 nozzle	9.3% D
Sduct-LaRC-46	LaRC BPR8 nozzle	4.6% D
Sduct-5BB-45	5BB	4.5% D

Seven vane configurations were modeled and analyzed: five for take-off conditions and two for cruise conditions. The vane configurations used the 5BB nozzle as their baseline. The vanes were simple NACA 0012 airfoils[16]. Each vane configuration had two pairs of vanes in the fan stream, an upper pair and a lower pair, and each vane has three parameters describing its orientation: angle of attack, azimuth angle (measured from the bottom), and axial position (measured forward of the fan stream nozzle exit). Table 2 lists out the parameters for each vane case. Figure 4 shows a rendering of the Vane_E take-off configurations.

Table 2: Vane configurations

Configuration	Baseline	Upper Vane			Lower Vane		
		AOA	Azimuth	Axial	AOA	Azimuth	Axial
Vane_A	5BB	5°	130°	0 chord	15°	50°	0 chord
Vane_B	5BB	5°	130°	¼ chord	12°	50°	¼ chord
Vane_C	5BB	5°	125°	¼ chord	8°	55°	¼ chord
Vane_D	5BB	5°	125°	½ chord	12°	55°	½ chord
Vane_E	5BB	7.5°	120°	½ chord	7.5°	60°	½ chord
Vane_cruise25	5BB	0°	125°	¼ chord	0°	55°	¼ chord
Vane_cruise75	5BB	0°	125°	¾ chord	0°	55°	¾ chord

The experimental tests performed in the Aeroacoustic Propulsion Lab only used configurations based on the 5BB nozzle at take-off conditions. Furthermore, of the configurations tested computationally, only the Sduct-5BB-45 and Vane_E configurations were included in the experimental tests; the Sduct_LaRC, Vane_A through Vane_D, and Vane_cruise configurations were only examined computationally. Even though only two of the 10 S-duct and vane configurations were tested experimentally, the computer simulations of the other configurations provided valuable insight into the performance and characteristics of S-duct and vane offset fan stream nozzles.

B. Flow Conditions

This paper will present analyses of the offset fan stream nozzles at two flight conditions: take-off and cruise. The jet engine typically produces more noise at take-off than during other stages of flight. This is because the engine is flying at its highest power rating and it is closest to observers on the ground. Noise is classified as either "flyer-over" or "sideline." Fly-over noise is heard by observers directly below the aircraft as it flies overhead, while sideline noise is heard by observers not directly under the aircraft's flight path. The purpose of offsetting the fan stream is to shield observers on the ground from jet noise at take-off. It is important to assess both the turbulence structure of the jet plume and the nozzle performance. If the performance penalty is too large, flying that nozzle configuration will be uneconomical and not adopted by aircraft and engine manufacturers, regardless of how well it reduces jet noise. The cruise condition is also examined. Nozzle performance, and not noise reduction, is the primary concern at cruise as the aircraft spends most of its time at cruise. Table 3 gives the take-off and cruise conditions used in this set of analyses.

Table 3: Nozzle flow conditions

		Take-off	Cruise
Core Stream	T_0 [° R]	1498	1421
	p_0/p_∞	1.42	2.19
Fan Stream	T_0 [° R]	640	509
	p_0/p_∞	1.62	2.56
Freestream	M_∞	0.28	0.8
	p_∞ [lb/in^2]	14.4	3.46
	T_∞ [° R]	529.67	394

C. Nozzle Grids

Multi-block, wall-packed grids were created for each nozzle configuration. Symmetry was exploited to reduce the number of grid points and computational requirements. The baseline 5BB nozzle

grid was a 2D axisymmetric grid. The baseline LaRC BPR8 nozzle grid was a 3D grid covering a 22.5° axial sector. The vane and S-duct nozzle grids were 3D 180° azimuth sectors. The grids extended roughly 3.3*D* radially outward from the nozzle centerline and over 40*D* downstream of the nozzle. Grid structure was kept similar between each of the 5BB nozzle-based grids and between each of the LaRC BPR8 nozzle-base grids, the only differences being where the configuration geometry differed. Figures 5 and 6 show the typical S-duct and vane nozzle grids; Figure 7 shows the grid around the vane. The grids consisted of multiple blocks to aid with parallelization on multiprocessor computers to reduce convergence time. The S-duct nozzle grids had about 9 million grid points and the vane nozzle grids had about 10 million grid points. The 5BB baseline and LaRC BPR8 baseline grids had about 82,000 and 1.5 million grid points, respectively.

D. Computational Strategy

All the computational analyses were performed using Wind[17-19] version 5. Wind is a general purpose, 3D Reynolds-Averaged Navier-Stokes (RANS) code, developed and managed by the NPARC Alliance. The NPARC Alliance is a partnership between NASA Glenn Research Center, USAF Arnold Engineering Development Center, and The Boeing Company. Wind has matured as a multi-zone, structured grid compressible flow solver, offering a variety of turbulence models. Previous studies[20,21] have shown the Menter SST turbulence model[22] to perform superior to Wind's other turbulence models for nozzle flows. Therefore, the SST turbulence model was used for all the analyses presented in this work.

The size of the nozzle grids required a large amount of computational power to obtain a converged solution. Two multiprocessor computer systems were used: a 12-processor SGI Origina3400 system; and a 19-node Linux cluster based on Intel Xeon processors. Grid sequencing was also used to reduce convergence time. The first grid sequence used ¼ the points in each grid direction (axial, height, azimuth), and the second grid sequence used ½ the points in each grid direction. This effectively reduced the grids to 1/64 and 1/8 of their original number of points, respectively. (The 2D baseline grids were only sequenced in two directions, reducing the sequenced grids to 1/16 and 1/4 the number of original grid points.) The third and final grid sequence used all the grid points. Convergence was determined once the change in integrated forces between successive iterations reduced to the order of 0.01%. The typical solution took five to ten days to adequately converge.

IV. Results

It is important to note that an iterative process took place with each offset stream nozzle type, S-duct and vanes. A configuration was produced, modeled, and analyzed, and the results were used to determine the next configuration. For the S-duct, only a few configurations were necessary. However, five take-off and two cruise configurations were needed for the vane nozzle. For ease of comparison, plots of each configuration will be shown together, with results from the corresponding baseline nozzle. The analysis of the results will attempt to narrate the iterative process that actually happened as each configuration was being computationally tested.

A. S-duct offset stream nozzles

In the early stages of the Offset Streams Technology task, it was not clear whether the 5BB nozzle or the LaRC BPR8 nozzle would be used as the baseline. The first offset stream nozzle configuration was the Sduct-LaRC-93 nozzle, which used the LaRC BPR8 nozzle as the baseline. Later, the decision was made to use the 5BB nozzle for experimental testing in the AAPL. This is why two of the S-duct nozzle configurations used the LaRC BPR8 nozzle, while all the other offset stream nozzle configurations presented here use the 5BB nozzle as the baseline.

1. *Take-off Flow Conditions*

The first S-duct nozzle tested with the Wind code was the Sduct-LaRC-93 nozzle, with the fan stream offset by 9.3% *D*. In Figure 8, contours of velocity are compared for the Sduct-LaRC-93 nozzle and the baseline LaRC BPR8 nozzle at take-off conditions. The velocity u is normalized by the mass-averaged velocity of the primary stream, u_{jet}. Whereas the potential core of the baseline breaks down around 7*D* downstream of the fan stream exit, the potential core of the Sduct-LaRC-93 nozzle breaks down only 2.5*D*

downstream of the fan stream exit. Contours of turbulence are shown in Figure 9. The turbulence k is normalized as follows:

$$k^* = \frac{k}{u_{jet}^2}$$

Offsetting the fan stream does provide some reduction of turbulence on the lower side of the Sduct-LaRC-93 nozzle when compared to the baseline nozzle, from a $(k^*)_{peak}$=0.0132 on the baseline to $(k^*)_{peak}$=0.0129 on the Sduct-LaRC-96 nozzle. However, the turbulence on the upper side of the jet plume is greatly increased over that of the baseline, from $(k^*)_{peak}$=0.0132 to $(k^*)_{peak}$=0.0290. The peak values of turbulence in the mixing region of the plume are listed in Table 4.

Table 4: Peak values of turbulence in the mixing region of the jet plume of S-duct nozzles.

Configuration	$(k^*)_{peak}$, lower	$(k^*)_{peak}$, upper
LaRC Baseline	0.0132	
Sduct-LaRC-93	0.0129	0.0290
Sduct-LaRC-46	0.0118	0.0213
5BB Baseline	0.0132	
Sduct-5BB-45	0.0118	0.0210

The discharge coefficient,

$$Cd = \frac{\dot{m}_{CFD}}{\dot{m}_{theory}},$$

and thrust coefficient,

$$Cfg = \frac{\left(F_{momentum} + F_{pressure} + F_{viscous}\right)_{CFD}}{\left(F_{momentum}\right)_{theory}},$$

were calculated to assess how the nozzle's actual mass flow compared to the ideal mass flow and how efficiently the nozzle produced thrust. Additionally, the product of the discharge coefficient and the thrust coefficient, *Cd*Cfg*, was computed. In a number of cases, an offset stream nozzle's mass flow was reduced from the baseline, and it still efficiently produced thrust. However, since the thrust coefficient is computed using the actual mass flow rather than the ideal mass flow, it is not a true measure of how the actual thrust compares to the ideal thrust. The product *Cd*Cfg* is used to better assess the nozzle's actual performance. Lastly, the thrust coefficient in the vertical direction, $(Cfg)_y$, was calculated to help understand how much flow turning was produced by each offset stream nozzle. Table 5 presents these performance quantities as differences from the baseline. The Sduct-LaRC-93 nozzle sees a 0.61% reduction in discharge and a 0.35% reduction in axial thrust, and a 0.94% reduction in the product of thrust and discharge, compared to the baseline. The Sduct-LaRC-93 nozzle produces a 2.9% increase in thrust in the vertical direction, due to the offset flow.

Table 5: Performance of S-duct nozzles relative to baseline nozzles at take-off flow conditions.
***Cd*=Dischage coefficient; *Cfg*=Thrust coefficient; $(Cfg)_y$=Thrust coefficient in vertical direction**

Configuration	$\Delta(Cd)$	$\Delta(Cfg)$	$\Delta(Cd*Cfg)$	$\Delta((Cfg)_y)$
LaRC Baseline	0.00%	0.00%	0.00%	0.00%
Sduct-LaRC-93	-0.61%	-0.35%	-0.94%	2.90%
Sduct-LaRC-46	-0.36%	-0.39%	-0.73%	1.38%
5BB Baseline	0.00%	0.00%	0.00%	0.00%
Sduct-5BB-45	0.50%	-0.18%	0.33%	1.47%

In an attempt to reduce the high amount of turbulence on the upper side of the Sduct-LaRC-93 nozzle and reduce the performance losses, the Sduct-LaRC-46 nozzle configuration was conceived by reducing the fan stream offset from 9.3% *D* to 4.6% *D*. Looking again at the velocity contour plots in Figure 8, the length of the potential core of the Sduct-LaRC-46 nozzle is not reduced from the baseline

nozzle results as much as the potential core of the Sduct-LaRC-93 nozzle, but it is still reduced in length from 7*D* to about 3.5*D*. The plot of turbulence in Figure 9 shows that the peak turbulence on the lower side of the jet plume is reduced a greater amount than with the Sduct-LaRC-93 nozzle, to $(k^*)_{peak}$=0.0118. The peak turbulence on the upper side of the jet plume is increased to $(k^*)_{peak}$=0.0213, still a dramatic increase over the baseline, but lower than that of the 9.3% *D* offset S-duct nozzle. From Table 5, the Sduct-LaRC-46 nozzle sees less reduction of mass flow than the Sduct-LaRC-93 nozzle, from ***Δ(Cd)=***-0.61% to ***Δ(Cd)=***-0.36%, and nearly the same reduction in thrust coefficient as the Sduct-LaRC-93 nozzle. The resulting product of discharge coefficient and thrust coefficient was 0.73% less than the LaRC baseline nozzle, which is 0.20% better than the Sduct-LaRC-93 nozzle. The vertical component of force of the Sduct-LaRC-46 nozzle is 1.38% larger than the baseline, about half that of the larger offset Sduct-LaRC-93 nozzle. Because of the lower overall performance loss and the lower increase in turbulence on the upper side of the jet plume than with the larger fan stream offset, a smaller offset was selected for the final hardware, which is the Sduct-5BB-45 nozzle.

The velocity contours and turbulence contours for the Sduct-5BB-45 nozzle are pictured in Figures 8 and 9, respectively, along with the corresponding contours for the 5BB baseline nozzle. As expected, the Sduct-5BB-45 nozzle produced peak turbulence levels comparable to the Sduct-LaRC-46 nozzle: $(k^*)_{peak}$=0.0118 on the lower side of the jet plume and $(k^*)_{peak}$=0.210 on the upper side of the jet plume. Additionally, the mass flow and thrust performance of the Sduct-5BB-45 nozzle see even less performance reduction than the Sduct_LaRC-46 nozzle. In fact, according to the data listed in Table 5, the Sduct-5BB-45 nozzle sees *increased* mass flow over the 5BB baseline nozzle by 0.50%. The Sduct-5BB-45 nozzle also produced thrust more efficiently than the previous two S-duct nozzles, suffering only 0.18% loss from its respective baseline. The resulting product of the mass and thrust coefficients is an increase over the baseline, by 0.33%. The vertical component of thrust of the Sduct-5BB-45 nozzle is on par with the Sduct-LaRC-46 nozzle, at 1.46% over the baseline.

Figure 10 and 11 show contours of velocity and turbulence at stations in the jet plume for each of the S-duct offset stream nozzles. Similar to what Papamoschou demonstrated for offset stream nozzles using vanes[10-13], the S-duct offset stream nozzles also significantly change the structure of the jet plume. Whereas the plumes of Papamoschou's vane nozzles resemble an upside-down pear – fat on the top and thin on the bottom -- the S-duct nozzle plumes resemble a right-side-up pear – fat on the bottom and thin on the top. This is probably because the S-duct nozzles pinch off more flow at the very top of the fan flow nozzle, directing more of the fan flow downward. In general, the S-duct offset stream nozzles flatten the core stream flow in the plume between *x/D*=1 and *x/D*=3, which is observed in Figure 10. The S-duct nozzles also create a horseshoe-shaped area of high turbulence on the upper side of the plume between *x/D*=3 and *x/D*=5, as observed in Figure 11. Additionally, the amount of offset in the S-duct impacts the plume shape, too: the greater offset of the Sduct-LaRC-93 nozzle more greatly resembles the right-side-up pear shape than the smaller offset S-duct nozzles.

2. Cruise Flow Conditions

It is generally known that airframe manufacturers will typically refuse any change if the overall performance of the aircraft is reduced more than 0.25%, regardless of the perceived benefit the change brings. Because the vast majority of the aircraft's flight is at cruise conditions, it would be difficult to justify a noise-reduction technique that reduces cruise performance beyond 0.25%. Therefore, analyses of the S-duct offset stream nozzles were also performed at cruise conditions. Velocity contours are plotted in Figure 12 and do not show any unexpected separations or strong shocks. The discharge and thrust coefficients relative to the baseline nozzle are listed in Table 6 for each S-duct nozzle. In general, the S-duct nozzles see fewer losses at cruise conditions than at take-off conditions. The Sduct-LaRC-93 nozzle sees a 0.27% reduction in mass flow and a 0.40% reduction in the thrust coefficient from the baseline nozzle, giving it an overall *Cd*Cfg* that is 0.69% smaller than the baseline. Surprisingly, the smaller offset S-duct nozzles perform nearly as well as the baseline nozzles at cruise conditions: the Sduct-LaRC-46 and Sduct-5BB-45 nozzles see virtually no change in the mass flow and nearly no change in the thrust coefficient from their respective baseline nozzles. The Sduct-LaRC-93 sees an increase in the vertical thrust by 2.65%, while the Sdut-LaRC-46 and Sduct-5BB-45 nozzles each see vertical thrust increased by about 1.4%. Even though only a small amount, the additional thrust in the vertical direction

could be desirable to an airframe manufacturer from the standpoint that less lift would be required from the wings, which typically equates to a reduction in drag.

Table 6: Performance of S-duct nozzles relative to baseline nozzles at cruise flow conditions. *Cd*=Dischage coefficient; *Cfg*=Thrust coefficient; $(Cfg)_y$=Thrust coefficient in vertical direction

Configuration	*Δ(Cd)*	*Δ(Cfg)*	*Δ(Cd*Cfg)*	$\Delta((Cfg)_y)$
LaRC Baseline	0.00%	0.00%	0.00%	0.00%
Sduct-LaRC-93	-0.27%	-0.40%	-0.69%	2.65%
Sduct-LaRC-46	0.01%	-0.06%	-0.07%	1.40%
5BB Baseline	0.00%	0.00%	0.00%	0.00%
Sduct-5BB-45	-0.01%	0.00%	0.01%	1.42%

B. Vane offset stream nozzles

Analyses were also completed on offset stream nozzle configurations using vanes to turn the fan flow downward. By the time the vane nozzles were being configured, the Offset Stream Technology group had decided to use the 5BB nozzle as the bypass-ratio 8 baseline. As mentioned previously, CFD analyses were performed on seven different vane nozzle configurations: five take-off configurations with the vanes angled downward to produce the offset stream effect; and two cruise configurations with the vanes angled parallel to the axis to reduce performance losses at cruise conditions.

1. Take-off Flow Conditions

The first offset stream nozzle with vanes examined was the Vane_A nozzle, with the upper set of vanes having a mild 5° angle of attack and the lower set of vanes having an aggressive 15° angle of attack (see Table 2 for more details). Figure 13 shows the velocity contours along the symmetry plane of the jet plume, and compares the Vane_A case with the 5BB baseline nozzle. The Vane_A configuration successfully directs the fan stream flow downward, to where it could produce a shielding effect. The primary jet potential core of the Vane_A configuration breaks down around 4.5*D* downstream of the fan stream exit, whereas the potential core of the 5BB baseline breaks down at roughly 7*D* downstream of the fan stream exit. Contours of turbulence are plotted in Figure 14 and show that the turbulence is reduced to $(k^*)_{peak}$=0.0123 on the lower side of the jet plume and increased to $(k^*)_{peak}$=0.0179 on the upper side of the jet plume, from $(k^*)_{peak}$=0.0132 in the 5BB baseline jet plume. The peak values of turbulence in the jet plume are listed in Table 7 for the vane offset stream nozzles.

Table 7: Peak values of turbulence in the mixing region of the jet plume of vane nozzle.

Configuration	$(k^*)_{peak}$, lower	$(k^*)_{peak}$, upper
5BB Baseline	0.0132	
Vane_A	0.0123	0.0179
Vane_B	0.0125	0.0174
Vane_C	0.0120	0.0174
Vane_D	0.0121	0.0166
Vane_E	0.0119	0.0176

Contours of velocity and turbulence plotted at stations along the jet plume are shown in Figures 15 and 16. The jet plume structure of the Vane_A configuration is rather different than that of the typical S-duct nozzle (Figures 10 and 11): just downstream of the nozzle, the vane configuration produces corners in the plume at the azimuth of each vane. Further downstream, the plume shape resembles an upside-down pear, with a fat and rounded upper side, and smaller and slender lower side. The vanes seem to push a portion the secondary flow directly downward, whereas the S-duct nozzles move more of the secondary flow to the lower side of the plume, creating a more rounded plume structure. In the plot of turbulence (Figure 16), a region of turbulence is seen inside the fan stream-freestream shear layer at *x/D*=0.5 and *x/D*=1.0. This turbulence is a result of the flow separating off the lower vane, angled at 15°. This is confirmed by the plots of Mach number and turbulence over the lower vane in Figure 17. While the CFD analyses do not definitively show that separation off the vanes will increase noise, they do show that the separation of the vane will dramatically reduce discharge and thrust performance. This is

evident in Table 8, where the Vane_A configuration is observed to experience a 1.6% loss in mass flow from the 5BB baseline case, a 2.3% loss in thrust, and a 3.79% loss in the product $Cd*Cfg$. These were the largest losses seen by any of the offset stream nozzles examined in this study. The vertical thrust component increased over 5% with the Vane_A configuration, which is the largest increase of this study.

Table 8: Performance of vane nozzles relative to baseline nozzles at take-off flow conditions. *Cd*=Dischage coefficient; *Cfg*=Thrust coefficient; $(Cfg)_y$=Thrust coefficient in vertical direction

Configuration	$\Delta(Cd)$	$\Delta(Cfg)$	$\Delta(Cd*Cfg)$	$\Delta((Cfg)_y)$
5BB Baseline	0.00%	0.00%	0.00%	0.00%
Vane_A	-1.63%	-2.30%	-3.79%	5.06%
Vane_B	-0.49%	-0.40%	-0.87%	4.71%
Vane_C	-0.49%	-0.24%	-0.53%	3.84%
Vane_D	-0.27%	-0.30%	-0.56%	4.16%
Vane_E	-0.39%	-0.35%	-0.72%	3.68%

Continuing forward with the vane offset stream nozzles, the Vane_B configuration placed the lower vanes at a smaller angle of attack: 12°. The plot of velocity along the symmetry plane in Figure 13 shows that the Vane_B configuration turns the secondary flow downward slightly less than the Vane_A configuration. However, the potential core breaks down sooner, at 4.2D downstream of the fan flow exit. Comparing the turbulence levels of the Vane_B nozzle with the Vane_A nozzle in Figure 14, one can see that the Vane_B nozzle produces noticeably smaller region of turbulence on the upper side of the plume. The peak values of turbulence on the lower side of the plume for the Vane_B nozzle is $(k^*)_{peak}$=0.0125. The reduction in turbulence of the Vane_B nozzle from the baseline is only slightly less than that of the Vane_A nozzle. Looking at the velocity and turbulence contours in the plume in Figures 15 and 16, it is observed that the plume of the Vane_B nozzle does not have as sharp of corners as the plume of the Vane_A nozzle. Additionally, the plume flow does not penetrate as far downward as with the Vane_A nozzle. Furthermore, the turbulence in the vicinity of the nozzle does not indicate a large amount of separation coming off either set of vanes. This is confirmed in the plots of the flow around the lower vane in Figure 17. However, there is still a significant amount of turbulence on the lower vane, which could indicate a small region of separation. Another concern is that lower vanes on both the Vane_A and Vane_B nozzles generated a non-trivial sized region of supersonic flow beginning near the leading edge of the vanes. While no shocks appear to be present, there exists the possibility that some change in conditions or some other small perturbation could produce shocks, leading to increased noise from the nozzle. Both features – separation and supersonic flow – could possibly increase noise, though this is not clear from the CFD analyses. The discharge coefficient and the thrust coefficient of the Vane_B nozzle were 0.49% and 0.40% less than the 5BB baseline nozzle (see Table 8). This results in $Cd*Cfg$ being reduced by 0.87% from the baseline. While the performance losses of the Vane_B nozzle were a large improvement over those of the Vane_A configuration, the thrust in the vertical direction is only slightly smaller than that of the Vane_A nozzle: 4.79% greater than the baseline. The mass flow and thrust losses were still quite significant, and further vane nozzle configurations were tested.

The Vane_C nozzle further reduced the angle of attack of the lower pair of vanes to 8° while keeping the upper vanes at 5° angle of attack. The goal was that the reduction in angle of attack would decrease separation and Mach number over the vane. The velocity contours along the symmetry plane plotted in Figure 13 look similar to those of the Vane_B configurations. As expected, the Vane_C configuration turns the jet plume downward less than the previous two vane nozzle configurations, because the lower vanes have a smaller angle of attack. The primary flow potential core breaks down 4.5D downstream for the configuration, slightly later than for the Vane_B configuration. Contours of turbulence plotted along the symmetry plane, pictured in Figure 14, show that the reduced vane angle of attack elongates the regions of turbulence on the upper and lower sides of the plume, as compared to the Vane_B configuration. Yet, the peak value of turbulence on the lower side of the plume is smaller for the Vane_C configuration than for the Vane_B configuration: $(k^*)_{peak}$=0.0120 versus $(k^*)_{peak}$=0.0125. On the upper side of the plume, the peak vales of turbulence are the same for the Vane_C and Vane_B

configurations, $(k^*)_{peak}$=0.0174. This is rather unexpected, as it was initially thought the turbulence on the lower side of the plume would see a greater reduction with a larger turning angle. Comparing the plots of plume cross section velocity and turbulence contours in Figures 15 and 16 for the Vane_C and Vane_B nozzle configurations shows that the smaller vane angle of the Vane_C nozzle does in fact turn the plume less. The contour plots of the Mach number and turbulence around the vanes in Figure 17 are as expected: because the lower vane of the Vane_C nozzle is at 8° angle of attack, the regions of supersonic flow and separated flow are smaller than those of the Vane_B nozzle, with a lower vane angle of 12°. Returning to Table 8, the discharge and thrust coefficients, it is observed that the Vane_C nozzle experiences a 0.49% reduction in mass flow, the same as the Vane_B nozzle. However, the Vane_C nozzle performs better than the Vane_B nozzle in thrust performance, suffering only 0.24% reduction, compared to the Vane_B's 0.40% reduction in thrust coefficient. As expected, the reduction in the product *Cd*Cfg* of the Vane_C nozzle is smaller than that of the Vane_B nozzle: a loss of 0.53% from the baseline, as compared to a loss of 0.87% for the Vane_B nozzle. The vertical component of thrust produced by the Vane_C nozzles was 3.84% of the total thrust.

The Vane_D nozzle investigates the effect of moving the vanes forward by using the same 5° and 12° vane angles of attack as the Vane_B nozzle. The vanes are moved ¼ chord further upstream in the nozzle, such that the trailing edge is ½ chord upstream of the secondary stream nozzle exit (see Table 2 for more details). The hope was that the Mach number could be reduced by moving the vane upstream in the nozzle, to a region where the nozzle flow has not yet accelerated to as high a Mach number. The velocity contours along the symmetry plane plotted in Figure 13 look similar to those of the Vane_B and Vane_C configurations. Even though the vanes of the Vane_D configuration are at the same angles of attack as those of the Vane_B configuration, the Vane_D nozzle appears to turn the flow downward slightly less than the Vane_B nozzle. This may be a result of moving the vanes upstream in the nozzle. Like the Vane_C nozzle, the primary flow potential core of the Vane_D nozzle breaks down 4.5*D* downstream of the secondary stream exit, about 0.3*D* later than the Vane_B nozzle. In the plots of turbulence in Figure 14, it is difficult to pick out any differences between the Vane_D and Vane_B configurations. On both the upper and lower sides of the jet plume, the peak values of turbulence for the Vane_D nozzle are less than those of the Vane_B nozzle: $(k^*)_{peak}$=0.0121 on the lower side and $(k^*)_{peak}$=0.0166 on the upper side, as compared to $(k^*)_{peak}$=0.0125 on the lower side and $(k^*)_{peak}$=0.0174 on the upper side for the Vane_B configuration. Therefore, moving the vanes upstream did affect the plume. The velocity and turbulence plume cross section plots in Figures 15 and 16 show some more differences between the Vane_D and Vane_B nozzles: at 0.5*D* and 1.0*D* downstream of the nozzle, the Vane_D configuration shows a reduction in the corner sharpness directly downstream of the vanes. Therefore, placing the vanes upstream in the nozzle creates a more rounded plume, while placing the vanes downstream in the nozzle creates a plume with sharper corners. Beyond 3.0*D* downstream of the nozzle, the Vane_D configuration does not penetrate downward as much as the Vane_B configuration, showing that moving the vanes upstream reduces the turning effect. The contour plots of the Mach number and turbulence around the vanes are shown in Figure 17. Compared to the Vane_B configuration, the Vane_D configuration has a smaller region of supersonic flow, as was expected. However, merely moving the vane upstream on the Vane_D configuration did not reduce the amount of separated flow as much as reducing the vane angle of attack did on the Vane_C configuration. In Table 8, it is observed that the discharge coefficient of the Vane_D nozzle only experiences a 0.27% decrease in mass flow from the baseline, as compared to a 0.49% decrease for the Vane_B nozzle. Similarly, the Vane_D nozzle sees only a 0.30% reduction in the thrust coefficient from the baseline, as compared to 0.40% for the Vane_B nozzle. The result is that the product *Cd*Cfg* for the Vane_D configuration is reduced by only 0.56% from that of the baseline, as opposed to 0.87% for the Vane_B configuration. However, the Vane_C nozzle performs better than the Vane_D nozzle in thrust performance, suffering only 0.24% reduction, compared to the Vane_D's 0.30% reduction in thrust coefficient. Moving the vanes forward did reduce the vertical component of thrust from 4.71% for the Vane_B nozzle to 4.16% for the Vane_D nozzle.

As with the S-duct offset stream nozzle, the primary objective of the CFD analyses of different vane offset stream nozzles was to determine hardware configurations for acoustics testing in the NASA Glenn Research Center AAPL. The Vane_A configuration showed that a vane angle of attack of 15° was

too high, producing separated flow, leading to performance losses and possibly increased noise. The Vane_B nozzle, with a 12° vane angle of attack, also showed signs of separated flow, but its performance did not suffer as greatly as the Vane_A nozzle. The Vane_C and Vane_D configurations produced good results, but by different methods: by further reducing the vane angle of attack; and by simply moving the vane upstream in the nozzle. In both cases, mass flow and thrust performance were improved and turbulence on the lower side of the plume was reduced. The Vane_E configuration (see Table 2) is similar to the Vane_C configuration, though now both sets of vanes have the same angle of attack, 7.5°. Looking at the velocity contours in Figure 13, the Vane_E configuration appears to direct the plume downward less than that of the other vane configurations. However, the primary flow potential core breaks down sooner than the Vane_B, Vane_C, and Vane_D nozzles, at x/D=4.4. The turbulence in Figure 14 looks very similar to that of the Vane_C and Vane_D cases. Even the values of peak turbulence are nearly equal with these two earlier configurations: $(k^*)_{peak}$=0.0119 on the lower side of the plume and $(k^*)_{peak}$=0.0176 on the upper side of the plume. The structure of the plume, as seen in Figures 15 and 16, looks slighty different for the Vane_E nozzle than for the Vane_C and Vane_D nozzles. The plume of the Vane_E nozzle is more rounded and has a larger amount of turbulence on the upper side at x/D=5.0 than the previous configurations. The flowfield around the lower vane in Figure 17 shows that the vane is free of supersonic flow and does not produce much turbulence. As observed in Table 8, the Vane_E configuration experiences a mass flow loss of 0.39% and a 0.35% loss in the thrust coefficient, resulting in a *Cd*Cfg* value reduced 0.72% from the baseline 5BB nozzle. It also produces a vertical thrust 3.86% of the total thrust of the 5BB nozzle.

There are three parameters for each pair of vanes: angle of attack, axial location, and azimuth angle. The five offset stream vane nozzles changed two – and sometimes all three – parameters between each iteration of nozzle design. Therefore, no conclusions about the effects of each parameter could be drawn directly. However, based upon the CFD analyses, it can be concluded that angle of attack has a large effect. The axial location of the vane also appears to have an effect, though smaller. It was inconclusive what effect was caused by the vane azimuth angle. As mentioned previously, jet rig testing was performed on a number of vane nozzle configurations in the NASA Glenn Research Center AAPL to better define the effects of the vanes, especially on the jet noise. The various configurations that were tested were determined through MDOE. The Vane_E nozzle configuration, while not the best performing of the vane nozzles, did perform well enough and is representative of the vane nozzles enough that it was used as the center point of the MDOE matrix of configurations. For more information regarding the MDOE matrix developed for the Offset Stream Technologies task experiments, the reader is invited to read discussion by Brown and Bridges[23].

2. Cruise Flow Conditions

As with the S-duct nozzles, CFD analyses were run for the vane nozzles at cruise conditions. However, one advantage the vane offset stream nozzle concept has over the S-duct nozzle concept is that the vanes can be rotated to a neutral position once the aircraft reaches its cruising altitude. This is because the offset stream shielding effect is only necessary during take-off and climb. Therefore, two vane nozzle cruise configurations were modeled and tested: the Vane_cruise25 nozzle had the vanes positions ¼ chord upstream of the fan nozzle exit, and the Vane_cruise75 nozzle had the vanes positioned ¾ chord upstream of the fan nozzle exit. Figure 18 shows plots of the velocity contours for the vane nozzle cruise configurations along the symmetry plane. The plumes of the two cruise vane nozzles look nearly identical to the baseline 5BB nozzle at cruise. It appears that the vanes have a minimal impact at 0° angle of attack. Plots of the velocity contours through the plume are shown in Figure 19 and show that the vanes do have a small effect on the plume structure. As with the take-off configurations, the plumes of the cruise configurations exhibit corners at the same azimuth locations as the vanes. The corners are more rounded as the vanes are moved upstream in the fan nozzle. Figure 20 shows that the flowfield around the vanes is free from any separations, shocks, supersonic regions of flow, and turbulence. The discharge and thrust coefficients for the cruise vane cases are listed in Table 9. The Vane_cruise25 nozzle sees a 0.21% reduction in mass flow from the baseline nozzle, while the Vane_cruise75 experiences a 0.09% reduction. Neither nozzle sees a real change in the thrust coefficient from the baseline. The product *Cd*Cfg* shows a reduction for each nozzle similar to what was scene in the discharge coefficient.

One thing the cruise configurations of the vane nozzles show is that the presence of the vanes at 0° angle of attack reduces only the mass flow of the nozzle. There is a small drag force on the vanes – 0.68% and 0.57% of the total thrust for the Vane_cruise25 and Vane_cruise75 nozzles, respectively – and based upon the discharge coefficients and thrust coefficients in Table 9, the drag force reduces the mass flow efficiency but not the thrust efficiency from the ideal. While the overall thrust is reduced due to the reduced mass flow, the thrust is not reduced because of some other nozzle inefficiency. As expected, since the vanes are angled at 0° angle of attack, there is zero thrust in the vertical direction.

Table 9: Performance of vane nozzles relative to baseline nozzle at cruise flow conditions.
***Cd*=Dischage coefficient; *Cfg*=Thrust coefficient; $(Cfg)_y$=Thrust coefficient in vertical direction**

Configuration	$\Delta(Cd)$	$\Delta(Cfg)$	$\Delta(Cd*Cfg)$	$\Delta((Cfg)_y)$
5BB Baseline	0.00%	0.00%	0.00%	0.00%
Vane_cruise25	-0.21%	0.00%	-0.21%	0.00%
Vane_cruise75	-0.09%	-0.01%	-0.10%	0.00%

C. Comparison with Experimental Data

The CFD analyses helped in the development of jet rig hardware by indicating which vane nozzle parameters were most important. Even though Wind has been validated for jet flows and shown to perform well when predicting the general flowfield, it is still of interest to compare the CFD predictions to experimental data. The experimental flowfield results were acquired for the 5BB baseline, Sduct-5BB-45, and Vane_E nozzles for M_∞=0.20, instead of M_∞=0.28, the value used for the previous CFD results. Therefore, one more CFD analysis was performed for each of the two nozzle configurations, adjusting the freestream inflow parameters to correspond to M_∞=0.20. Contours of velocity for the CFD solutions and experimental particle image velocity (PIV) data are compared in Figures 21-23. It should be noted that the plots of PIV data do not include data of poor quality[23]. This explains why there are blank or white areas around the jet plumes and even inside the jet plumes. Therefore, the CFD solutions are being compared only to the higher quality PIV data. The CFD solution of the 5BB baseline nozzle shows excellent agreement with the PIV velocity data through most of the plume. The only exception is that the CFD solution delays the breakdown of the potential core in the region 5*D* to 7*D* downstream of the fan nozzle exit. This is not an isolated occurrence of this problem, but rather a known limitation of the RANS-based solutions for a number of turbulence model[24]. The CFD predictions of velocity for the S-duct and vane nozzles compare very well to the PIV data, matching in magnitude and structure. Contours of turbulence in the plume are compared between the CFD solutions and PIV data in Figures 24-26. The CFD solutions do a good job of predicting the structure of the turbulence in the plume. The only major disagreement observed is that the CFD does not predict the corners in the vane plume to be as sharp as what the PIV data shows. In addition to prolonging the breakdown of the jet potential core, the CFD solutions predict the peak levels of turbulence to be smaller than what is observed in the PIV data. This has been found to be problematic for computational aeroacoustics (CAA) analyses[15], as jet noise is directly related to the turbulence.

V. Conclusion

This work has detailed the results of CFD simulations of Offset Stream nozzles, presenting the results of nine nozzle configurations run at take-off conditions and five nozzle configurations run at cruise conditions. The findings were quite positive: S-duct and vane offset fan stream technologies reduced the amount of turbulence on the lower side of the jet plume. This was accomplished with less than a half percent reduction in the nozzle mass flow and thrust performance at take-off conditions. At cruise conditions, these losses were reduced to less than 0.1% for the later S-duct and vane configurations. The analyses showed that turbulence was reduced on the lower side of the jet plume, with peak values of turbulence being reduced by up to 11% for the S-duct nozzles and up to 10% for the vane nozzles. However, turbulence levels were significantly increased on the upper side of the plume: by nearly 60% for the later S-duct nozzles and 33% for the vane nozzles. Because it is the thickening of the lower side of the plume that provides an acoustical shielding effect to observers on the ground below, the increased

turbulence levels on the upper side of the plume should not be a problem. The vane configurations produced a larger jet turning effect than the S-duct configurations, resulting in a vertical component of thrust three to four times greater at take-off conditions.

Because this work was performed in preparation of experimental work, care was taken to try to determine the effects of varying different parameters for each of the vane and S-duct offset fan stream technologies. For the S-duct configurations, it was observed that a moderate amount of fan stream offset produced less turbulence on the lower side of the jet plume and reduced thrust and mass flow performance less than a larger offset of the fan stream. On the vane nozzle configurations, vane angles of 12° and greater produce separated flow and supersonic regions of flow near the vanes. While it is currently unclear whether supersonic flow over vanes (with or without shocks) contributes to jet noise, it is clear that separated flow does reduce performance and produces turbulence in the jet plume. However, moving the vanes forward in to the nozzle flow reduced flow separation and the amount of supersonic flow over the vane. Varying the azimuth angle of the vanes showed no significant changes in turbulence or performance. These observations were incorporated into developing the test matrix and configurations of the S-duct and vane nozzles for testing in the NASA Glenn Research Center AAPL.

It was noted that the structure of the jet plumes differed between the S-duct and the vane nozzles. Looking at cross sections of the plume, the S-duct nozzles did a better job of offsetting the fan stream with respect to the core stream, as the plume was rounder and fuller on the bottom. In contrast, the vanes merely pushed a portion of the fan stream downward. The plume of the vane nozzle was less full on the sides than the plume of the S-duct nozzle. Furthermore, the jet plumes observed by Papamoschou[10-13] in his experiments with vane nozzles show more similarities with the S-duct nozzles analyzed here than the vane nozzles. This is because the S-duct nozzles and Papamoschou's vane nozzles are full and round on the lower side. One possible reason for the dissimilarity between these two sets of vane nozzle plumes is that the nozzle geometries were different: the 5BB nozzle used in the current study had a plug, had fan and core streams exit at different axial locations, and had fan and core streams directed towards the axis rather than parallel to the axis. The nozzle used by Papamoschou had no plug, had fan and core streams exit at the same axial plane, and had fan and core streams directed parallel to the axis. The plumes of the vane Offset Stream nozzles also developed corners, directly downstream of the vanes, even when the vanes had zero angle of attack. The corners were more pronounced as the vanes were moved downstream. It is not known whether these corners in the jet plume affect the noise, but they do not appear to increase turbulence.

The vanes used in the vane offset stream nozzles were based upon the NACA 0012 airfoil. While the NACA 0014 airfoil has been used for many years as a test airfoil, it is well know that it is not an optimum transonic airfoil, and this study clearly shows that the vanes see transonic flow in the fan stream nozzle. Further improvements could be made in both nozzle performance and noise reduction if the airfoil section were optimized. Using a modern transonic airfoil should reduce separation, reduce the risks of shocks, and decrease turbulence on the vanes – all factors that impact performance. In fact, with the selection of an optimized airfoil, it should be possible to increase the vane angle of attack without suffering separation, thus producing a greater shielding effect and larger noise reduction than observed in this study. While a symmetrical airfoil section is not a requirement, a symmetrical airfoil could easily rotate to a zero-lift (zero angle of attack) configuration for cruise.

The computational analyses presented here proved to be invaluable in several ways. They allowed a number of different configurations to be tested before hardware was manufactured. This allowed well-performing designs to be selected over poor performing designs and costs to be reduced. The CFD analyses also allowed for the observation and prediction of nozzle flow characteristics that could not be observed in the experimental test, such as flow over and skin friction on the vanes and mass flow and thrust performance. The analyses demonstrated that S-duct and vane offset fan stream technologies are viable and do not greatly reduce performance. Lastly, the CFD results will be used as input to a jet noise prediction code[15], so that the jet noise prediction code can be validated against experimental noise measurements taken of the S-duct and vane nozzles

The Wind CFD analyses generally showed good agreement with the PIV data. The only exception to this was that the CFD solutions predicted a longer potential core in the jet than that which

was observed experimentally. The delayed breakdown of the potential core reduced the peak values of turbulence observed in the jet plume. This is a problem that all RANS solvers suffer, and can be anticipated when one is running CFD solutions. Other than this one area of disagreement, the rest of the jet plume – the velocity levels and plume structure – showed good agreement.

VI. Acknowledgements

The authors wish to acknowledge the Quiet Aircraft Technology program for funding this research effort. Additional gratitude is given to Nicholas Georgiadis, Jim Debonis, Dennis Yoder, and Charlie Towne for their input and guidance and to James Bridges and Cliff Brown for providing the experimental flow data.

VII. References

[1] Callender, B., Gutmark, R., and Martens, S., "A Far-Field Investigation into Chevron Nozzle Mechanisms and Trends," AIAA Paper 2003-1058, 2003.

[2] Callender, B., Gutmark, R., and Martens, S., "A Near-Field Investigation into Chevron Nozzle Mechanisms," AIAA Paper 2003-3210, 2003.

[3] Callender, B., Gutmark, R., and Martens, S., "A PIV Flow Field Investigation of Chevron Nozzle Mechanisms," AIAA Paper 2004-191, 2004.

[4] Bridges, J. and Brown, C. A., "Parametric Testing of Chevrons on Single-flow Hot Jets," AIAA Paper 2004-2824, 2004.

[5] Koch, L. D., Bridges, J., and Khavaran, A., "Mean Flow and Noise Prediction for a Separate Flow Jet with Chevron Mixers," AIAA Paper 2004-189, 2004.

[6] Engblom, W., Khavaran, A., and Bridges, J., "Numerical Prediction of Chevron Nozzle Noise Reduction using WIND-MGBK Methodology," AIAA Paper 2004-2979, 2004.

[7] Loheac, P., Julliard, J., and Dravet, A., "CFM56 Noise Reduction with the Chevron Nozzle," AIAA Paper 2004-3044, 2004.

[8] Calkins, F. T. and Butler, G. W., "Subsonic Jet Noise Reduction Variable Geometry Chevron," AIAA Paper 2004-190, 2004.

[9] Mabe, J. H., Cabell, R. H., and Butler, G. W., "Design and Control of a Morphing Chevron for Takeoff and Cruise Noise Reduction," AIAA Paper 2005-2889, 2005.

[10] Papamoschou, D. and Debiasi, M., "Mach Wave Elimination Applied to Turbofan Engines," AIAA Paper 2002-0368, 2002.

[11] Papamoschou, D., "A New Method for Jet Noise Reduction in Turbofan ," AIAA Paper 2003-1059, 2003.

[12] Papamoschou, D. and Nishi, K., "Jet Noise Suppression with Fan Flow Deflectors in Realistic-Shaped Nozzle," AIAA Paper 2005-993, 2005.

[13] Papamoschou, D., "Parametric Study of Fan Flow Deflectors for Jet Noise Suppression," AIAA Paper 2005-2890, 2005.

[14] Zaman, K. B. M. Q., "Noise- and flow-field of jets from an eccentric coannular nozzle," AIAA Paper 2004-5, 2004.

[15] Khavaran, A., Bridges, and Georgiadis, N., "Prediction of Turbulence-Generated Noise in Unheated Jets: Part 1: JeNo Technical Manual (Version 1.0)," NASA/TM-2005-213827, 2005.

[16] Abbot, I. H. and von Doenhoff, A. E., *Theory of Wing Sections: Including a Summary of Airfoil Data*, Dover Publications, 1959.

[17] Bush, R. Power, G., and Towne, C., "WIND: The Production Flow Solver of the NPARC Alliance," AIAA Paper 98-0935, 1998.

[18] Nelson, C. C. and Power, G. D., "CHSSI Project CFD-7: The NPARC Alliance Flow Simulation System," AIAA Paper 2001-0594, 2001.

[19] *The Wind User's Guide*, User Manual, The NPARC Alliance, http://www.grc.nasa.gov/WWW/winddocs/user/index.html.

[20]Georgiadis, N. and Papamoschou, D., "Computational Investigations of High-Speed Dual-Stream Jets," AIAA Paper 2003-3311, 2003.

[21]Georgiadis, N. J., Rumsey, C. L., Yoder, D. A., and Zaman, K. B. M. Q., "Effects of RANS Turbulence Modeling on Calculation of Lobed Nozzle Flowfields," AIAA Paper 2003-1271, 2003.

[22]Menter, F. R., "Two-Equation Eddy Viscosity Turbulence Models for Engineering Applications," AIAA Journal, Vol. 32, No. 8, pp. 1598-1605, 1994.

[23]Brown, C. and Bridges, J., "Offset Stream Technologies Test - Summary of Results," AIAA paper 2007-3664, 2007.

[24]Georgiadis, N. J., Rumsey, C. L., Yoder, D. A., and Zaman, K. B. M. Q., "Effects of RANS Turbulence Modeling on Calculation of Lobbed Nozzle Flowfields," 41st AIAA Aerospace Sciences Meeting and Exhibit, AIAA 2003-1271, Jan. 2003.

VIII. Figures

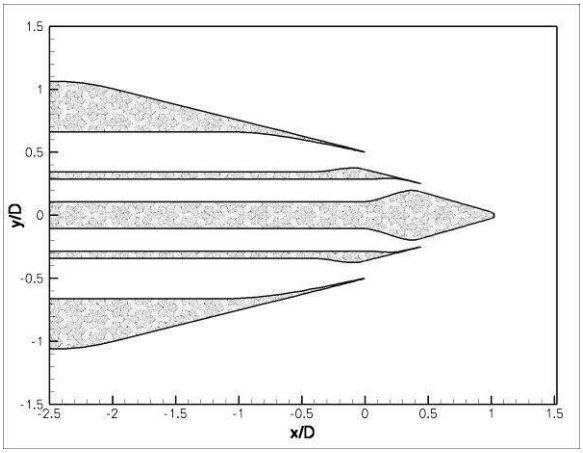

(a) LaRC BPR8 dual-flow nozzle.

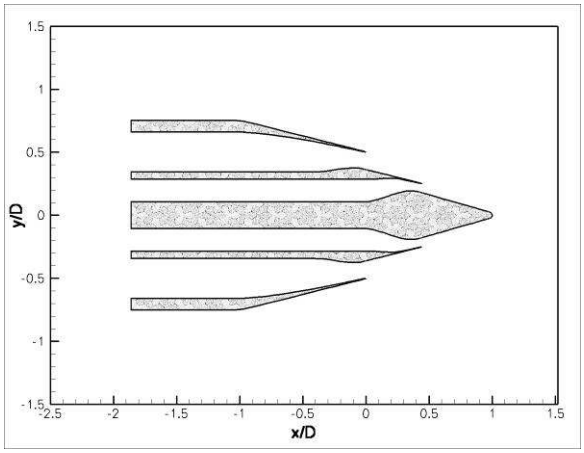

(b) 5BB dual-flow nozzle.

Figure 1: Flowlines of baseline nozzles.

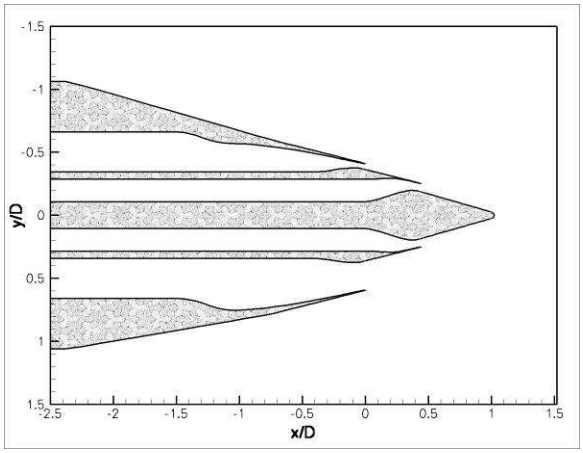

(a) Sduct-LaRC-93 nozzle.

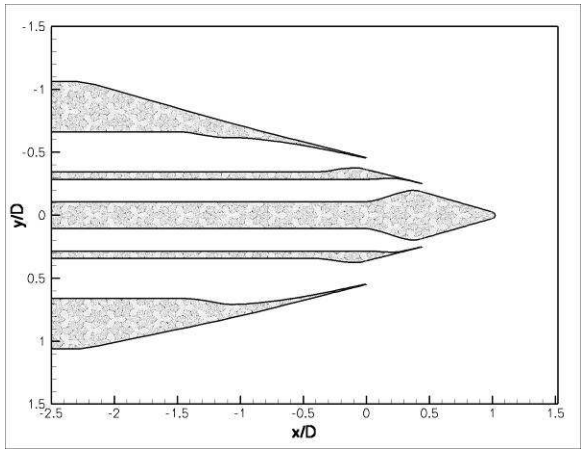

(b) Sduct-LaRC-46 nozzle.

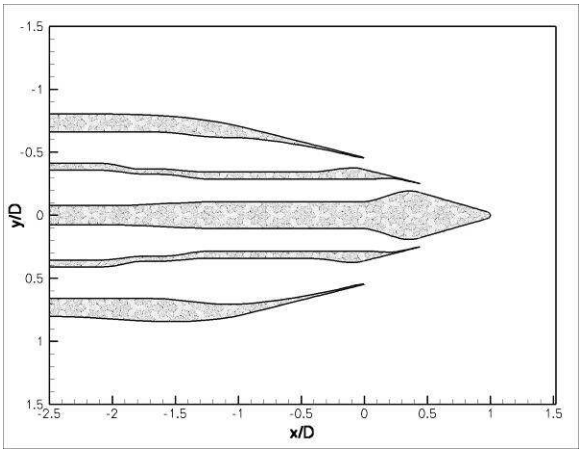

(c) Sduct-5BB-45 nozzle.

Figure 2: Flowlines for S-duct offset stream nozzles.

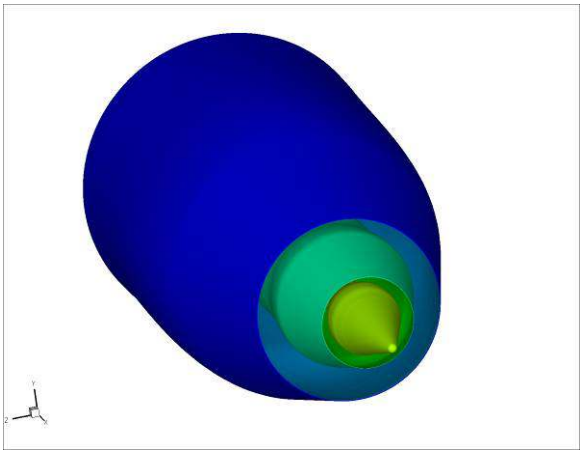

Figure 3: Rendering of Sduct-5BB-45 offset stream nozzle.

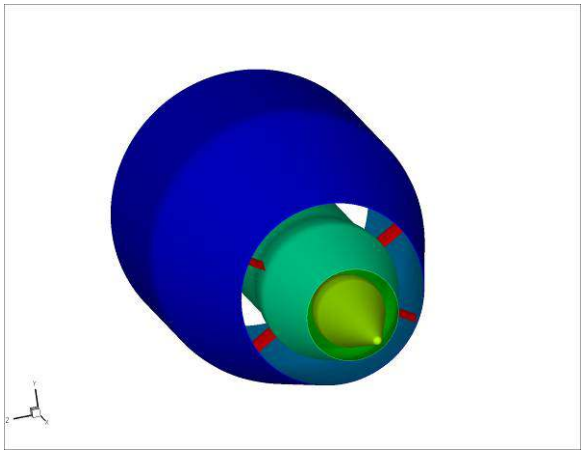

Figure 4: Rendering of Vane_E offset stream nozzle.

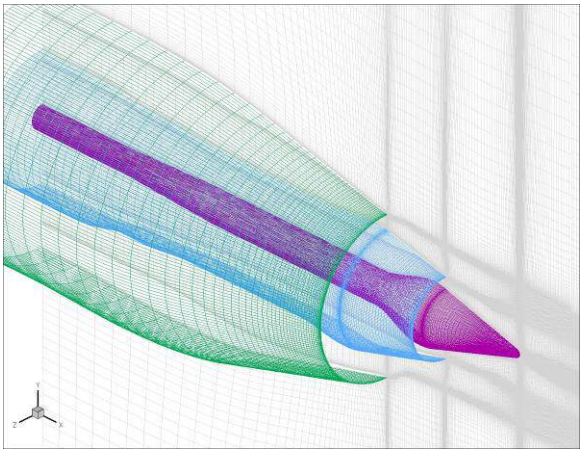

Figure 5: Grid around Sduct-5BB-45 offset stream nozzle.

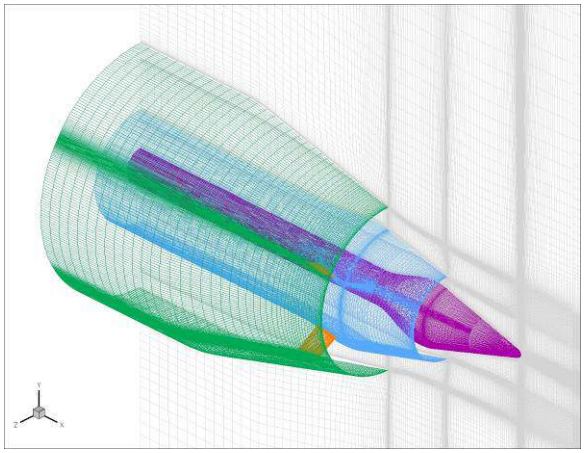

Figure 6: Grid around Vane_E offset stream nozzle.

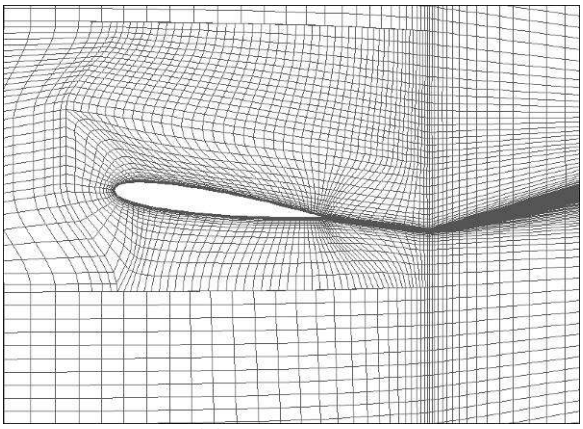

(a): Upper vane.

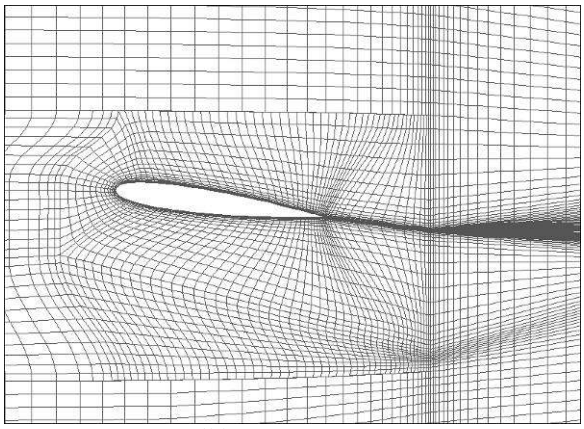

(b) Lower vane.

Figure 7: Grid around vanes of Vane_E offset stream nozzle.

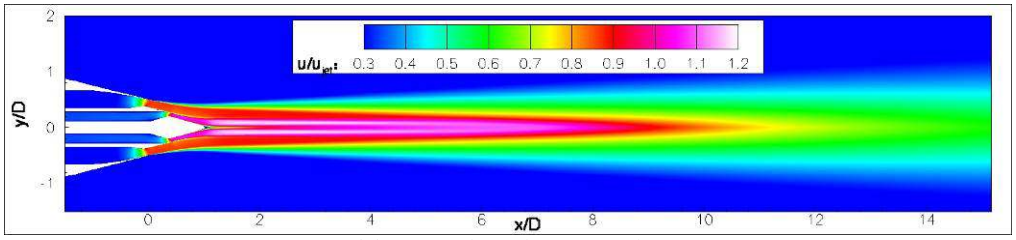

(a) LaRC baseline nozzle.

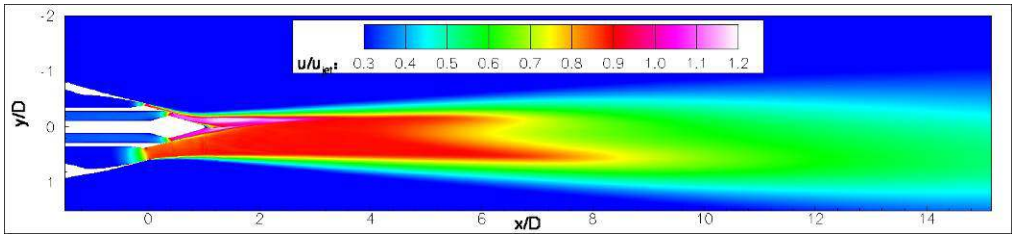

(b) Sduct-LaRC-93 nozzle.

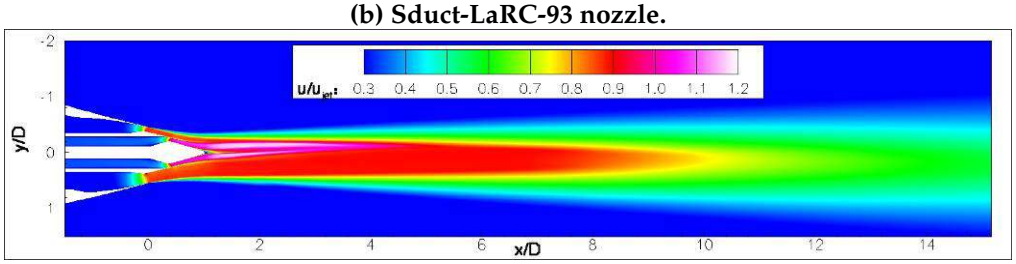

(c) Sduct-LaRC-46 nozzle.

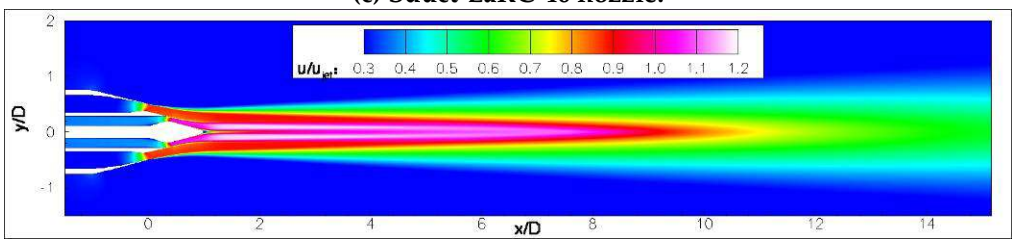

(d) 5BB baseline nozzle.

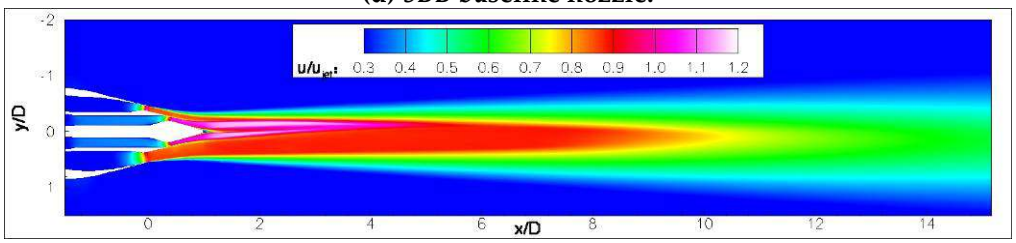

(e) Sduct-5BB-45 nozzle

Figure 8: Velocity contours on symmetry plane of S-duct nozzles and baselines at take-off flow conditions.

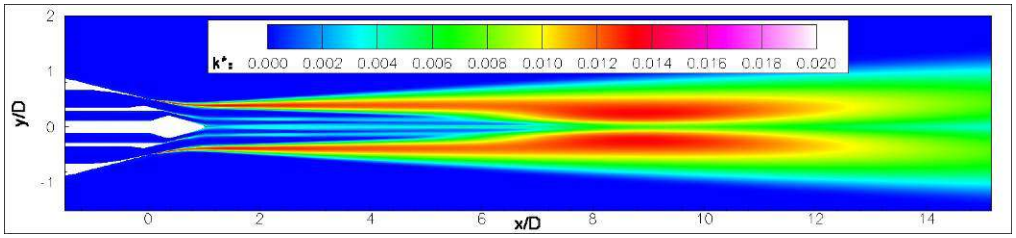

(a) LaRC baseline nozzle.

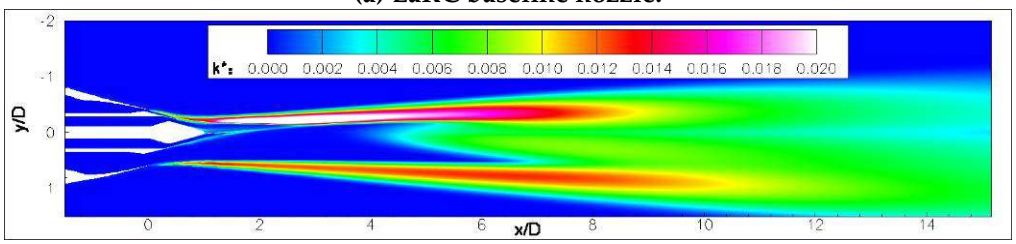

(b) Sduct-LaRC-93 nozzle.

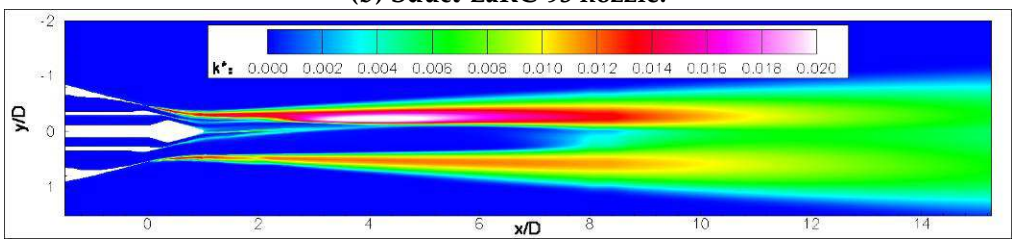

(c) Sduct-LaRC-46 nozzle.

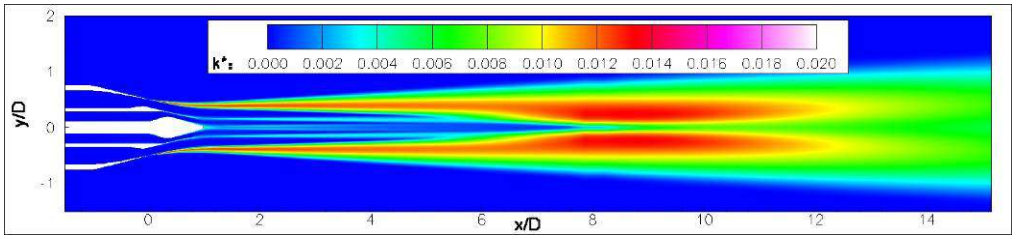

(d) 5BB baseline nozzle.

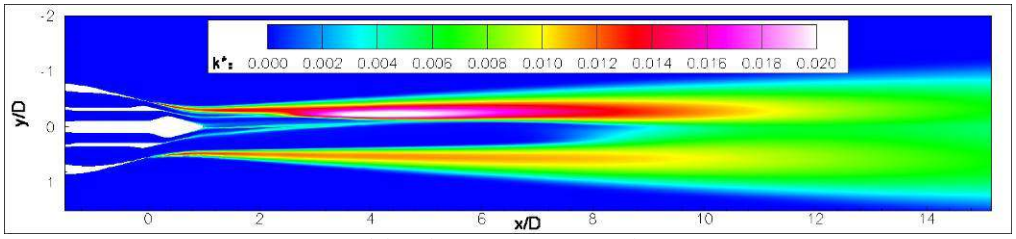

(e) Sduct-5BB-45 nozzle

Figure 9: Turbulence contours on symmetry plane of S-duct nozzles and baselines at take-off flow conditions.

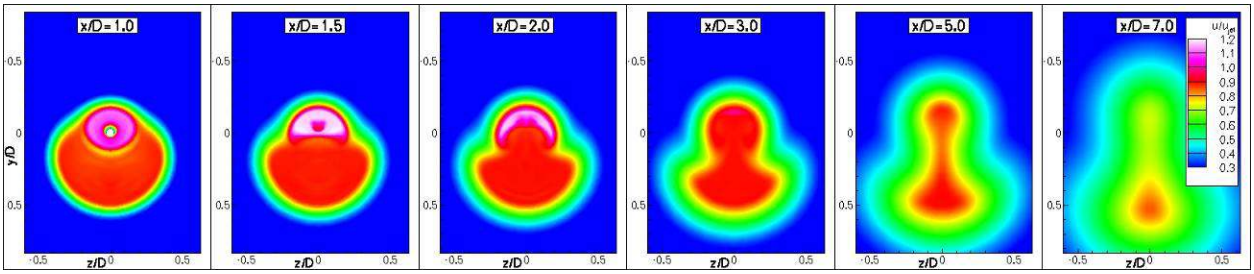

(a) Sduct-LaRC-93.

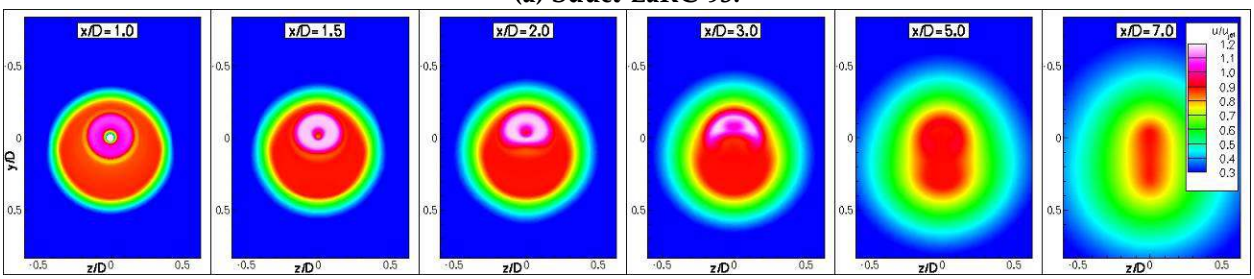

(b) Sduct-LaRC-46.

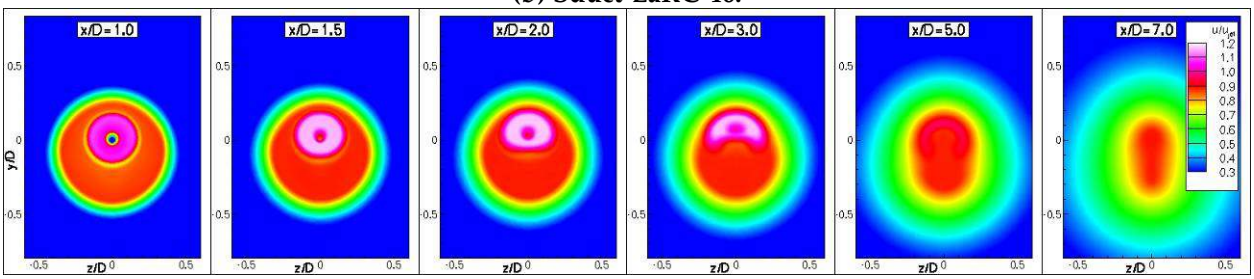

(c) Sduct-5BB-45.

Figure 10: Velocity contours at plume cross-sections of S-duct nozzles and baselines at take-off flow conditions.

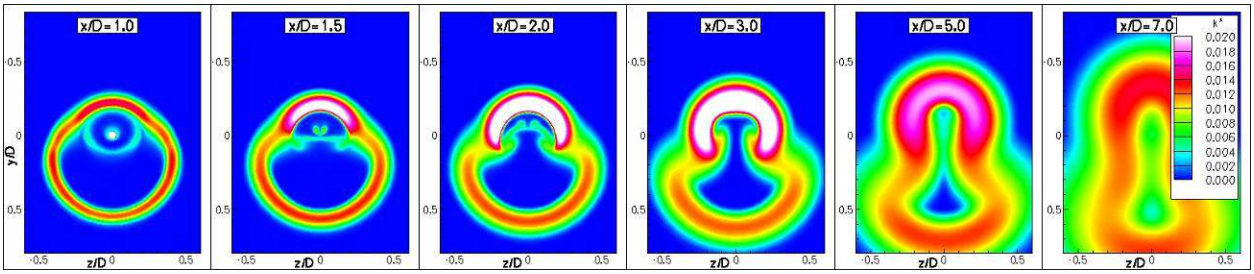

(a) Sduct-LaRC-93.

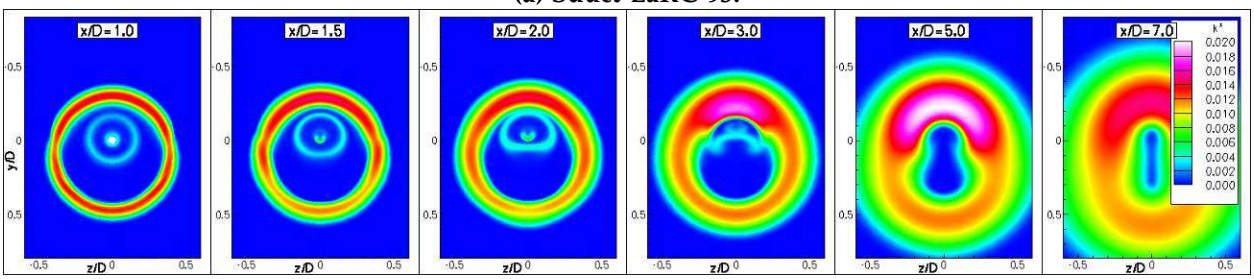

(b) Sduct-LaRC-46.

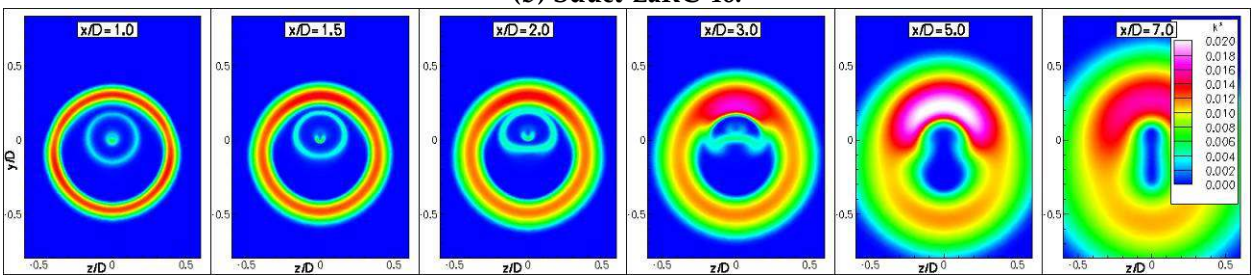

(c) Sduct-5BB-45.

Figure 11: Turbulence contours at plume cross-sections of S-duct nozzles and baselines at take-off flow conditions.

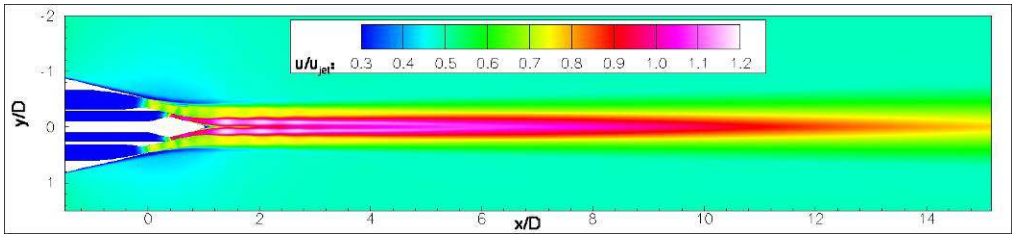

(a) LaRC baseline nozzle.

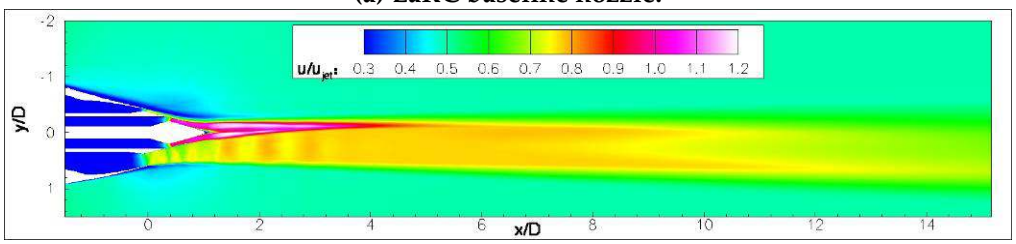

(b) Sduct-LaRC-93 baseline nozzle.

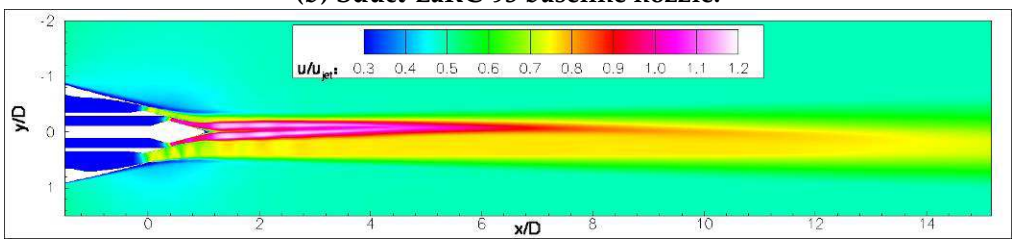

(c) Sduct-LaRC-46 baseline nozzle.

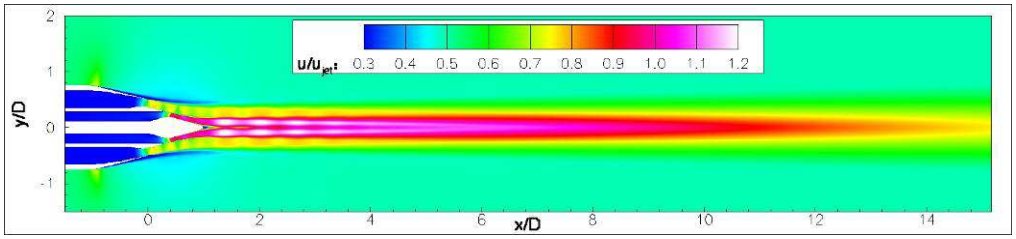

(d) 5BB baseline nozzle.

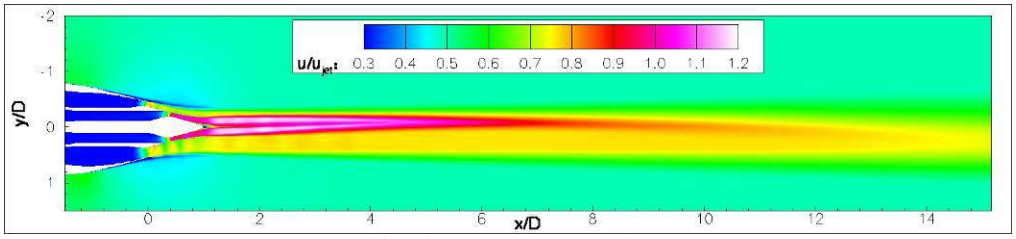

(e) Sduct-5BB-45 nozzle.

Figure 12: Velocity contours on symmetry plane of S-duct nozzles and baselines at cruise flow conditions.

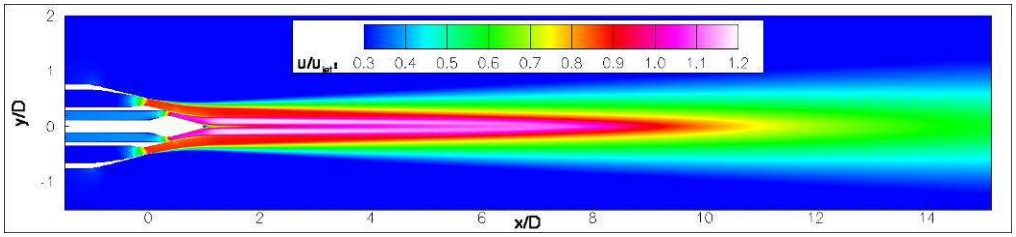

(a) 5BB baseline nozzle.

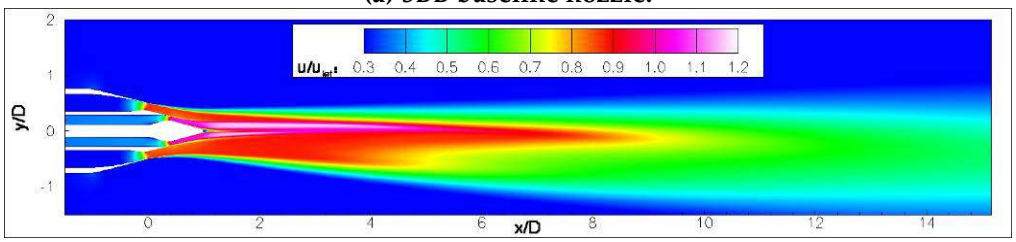

(b) Vane_A nozzle.

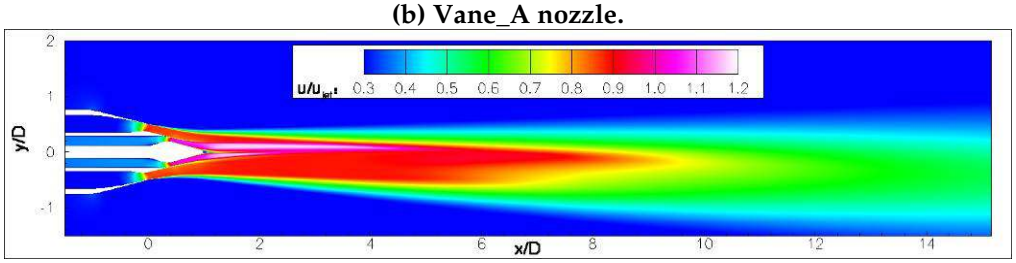

(c) Vane_B nozzle.

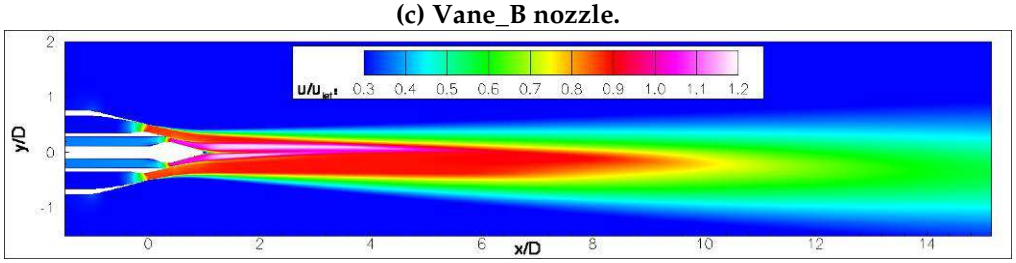

(d) Vane_C nozzle.

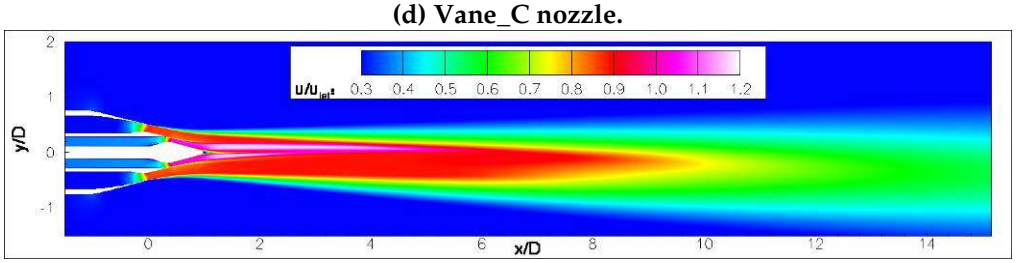

(e) Vane_D nozzle.

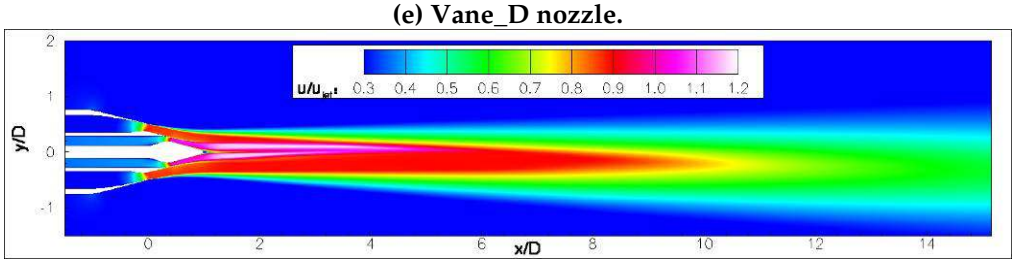

(f) Vane_E nozzle.

Figure 13: Velocity contours along symmetry plane of vane offset stream nozzles at take-off flow conditions.

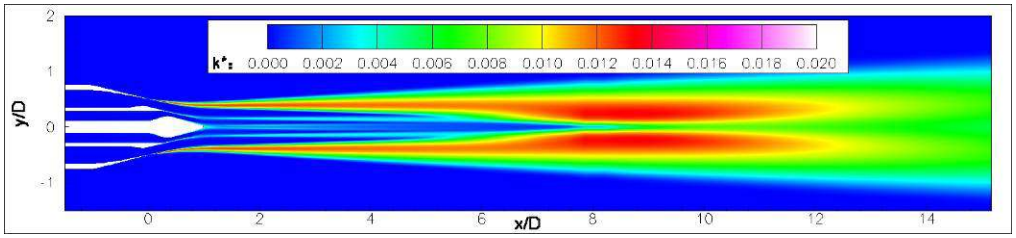

(a) 5BB baseline nozzle.

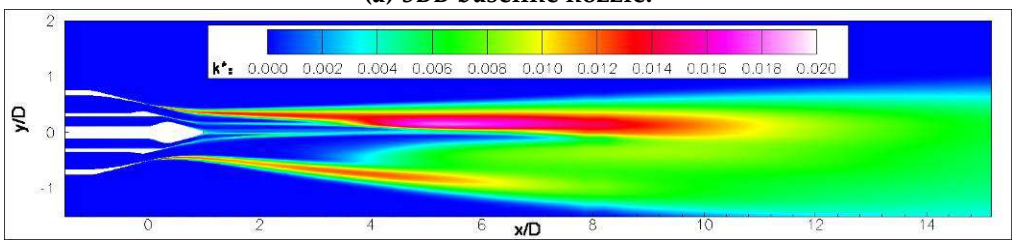

(b) Vane_A nozzle.

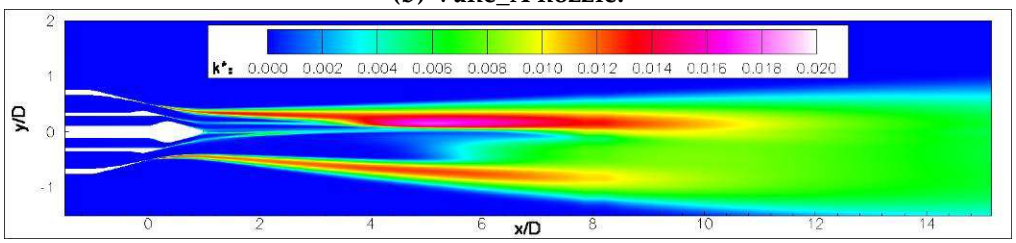

(c) Vane_B nozzle.

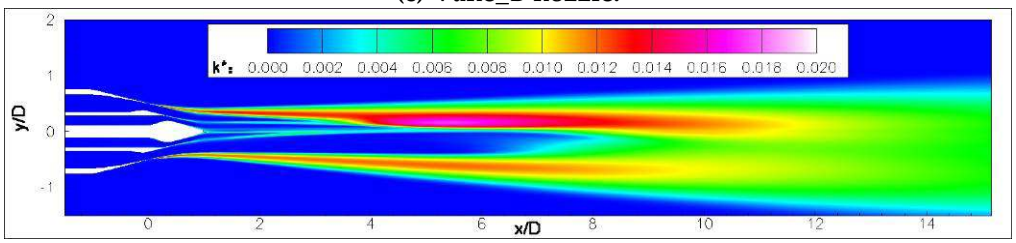

(d) Vane_C nozzle.

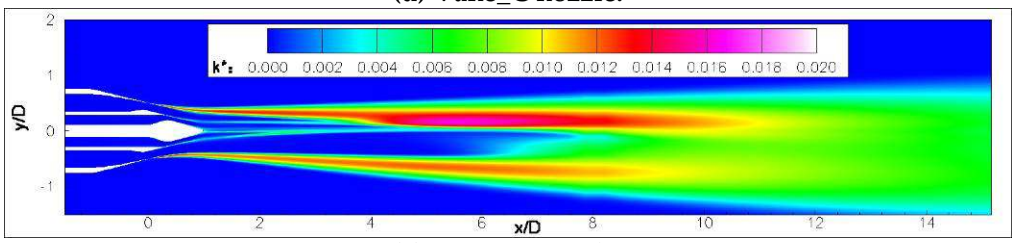

(e) Vane_D nozzle.

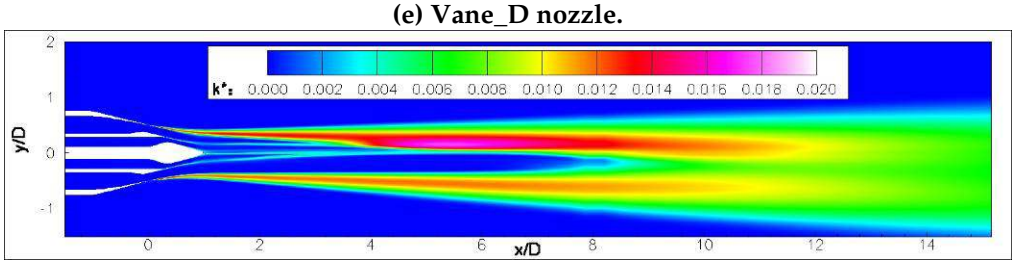

(f) Vane_E nozzle.

Figure 14: Turbulence contours along symmetry plane of vane offset stream nozzles at take-off flow conditions.

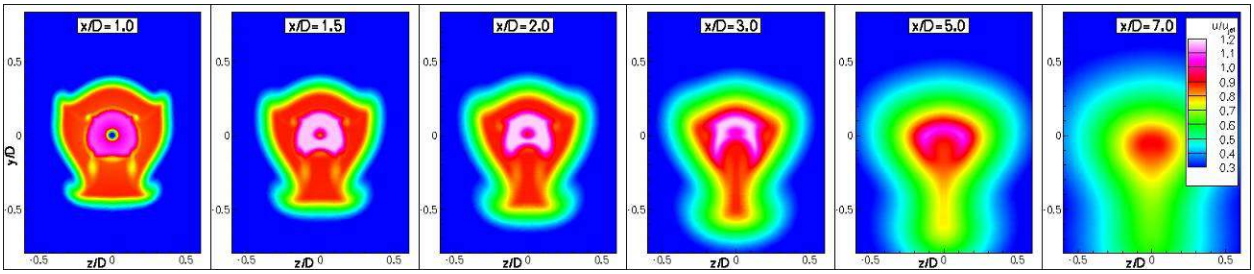

(a) Vane_A nozzle.

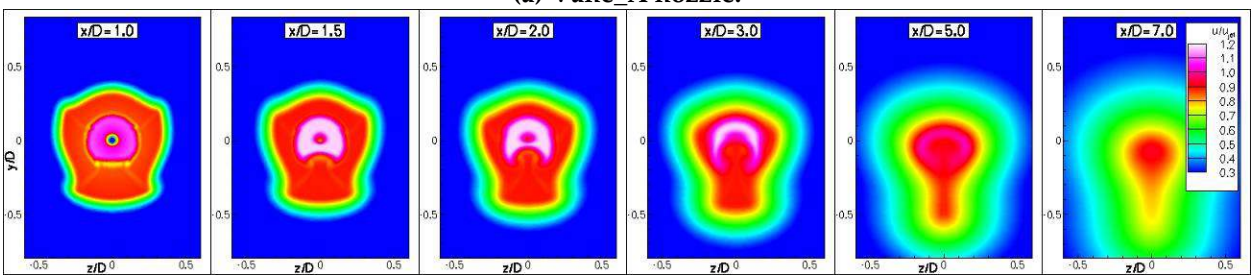

(b) Vane_B nozzle.

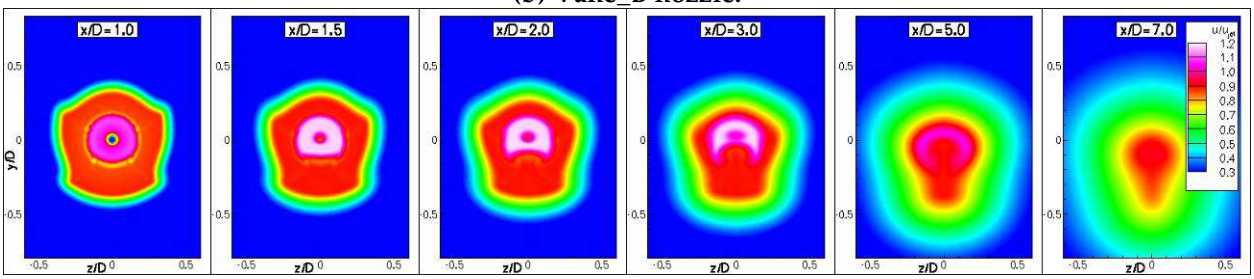

(c) Vane_C nozzle.

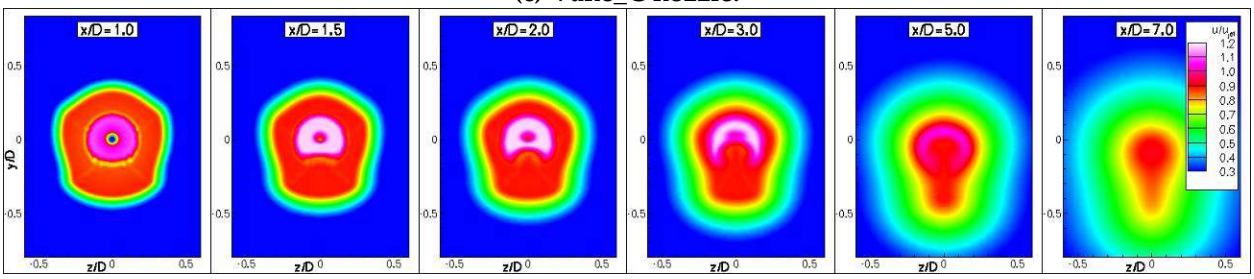

(d) Vane_D nozzle.

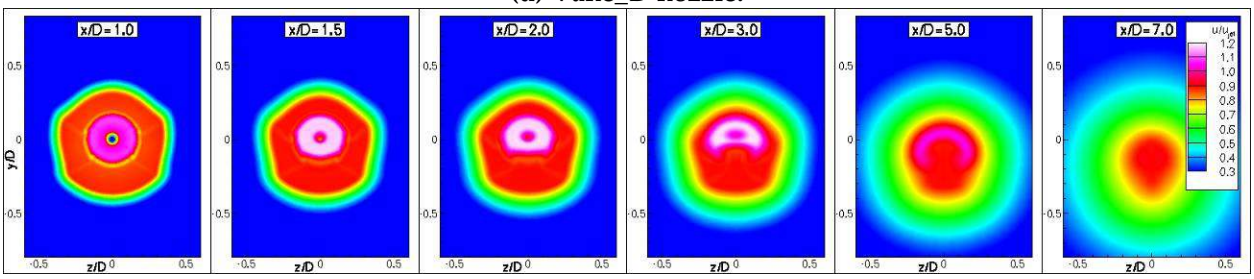

(e) Vane_E nozzle.

Figure 15: Velocity contours at plume cross sections of vane offset stream nozzles at take-off flow conditions.

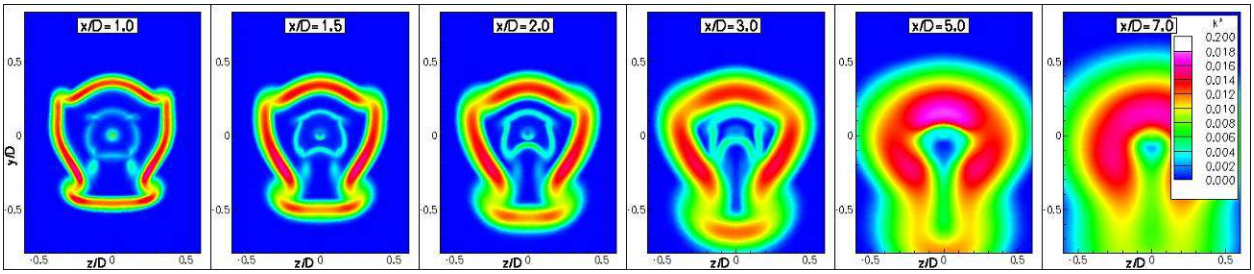

(a) Vane_A nozzle.

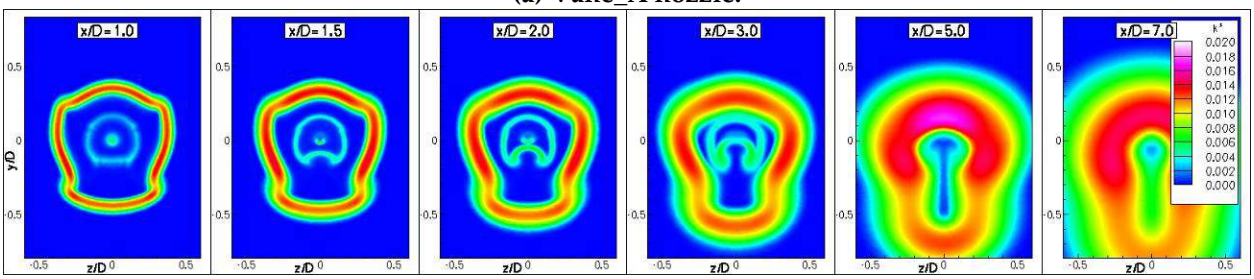

(b) Vane_B nozzle.

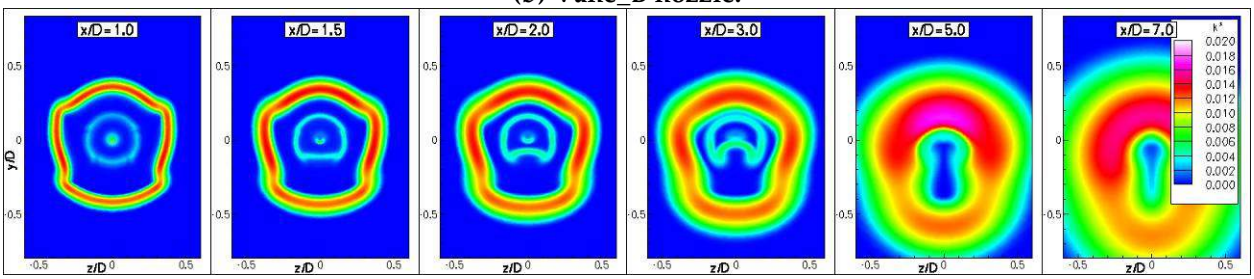

(c) Vane_C nozzle.

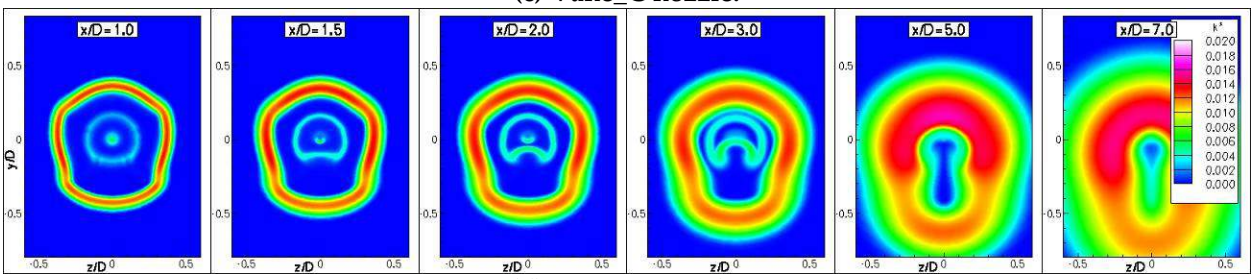

(d) Vane_D nozzle.

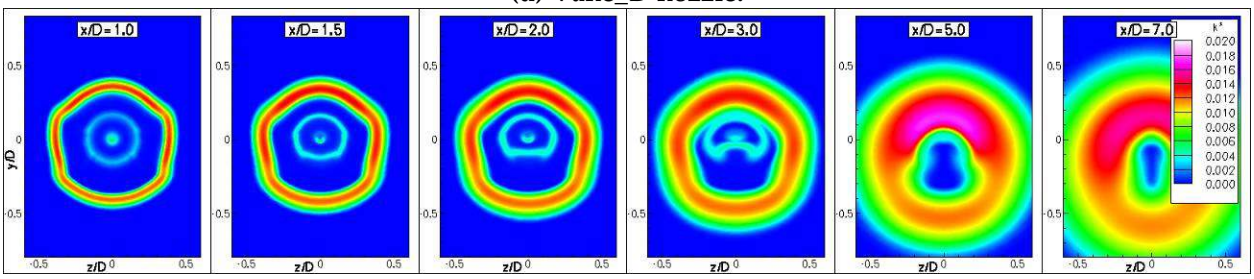

(e) Vane_E nozzle.

Figure 16: Turbulence contours at plume cross sections of vane offset stream nozzles at take-off flow conditions.

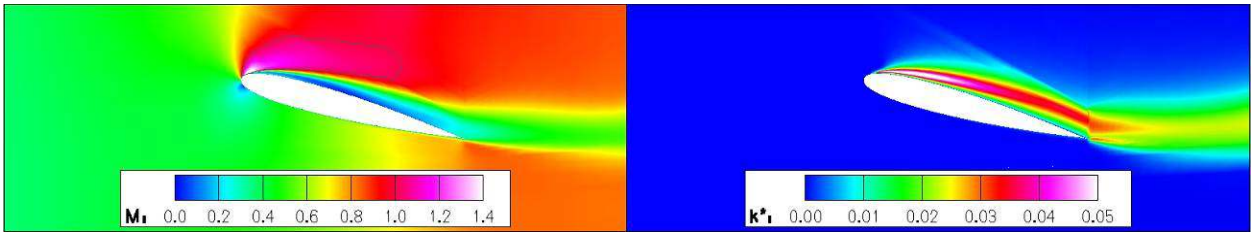

(a) Vane_A nozzle.

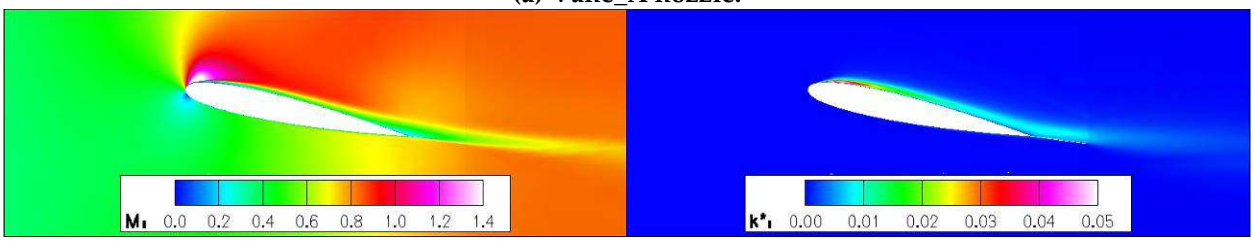

(b) Vane_B nozzle.

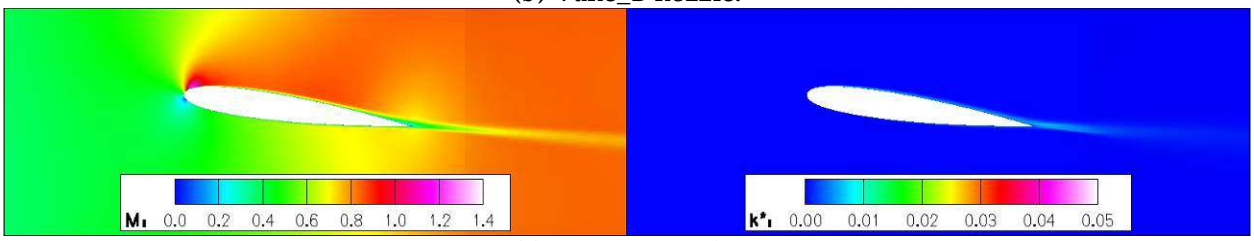

(c) Vane_C nozzle.

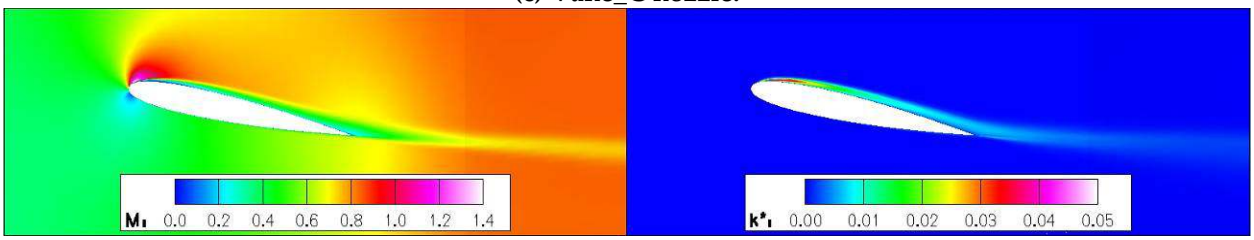

(d) Vane_D nozzle.

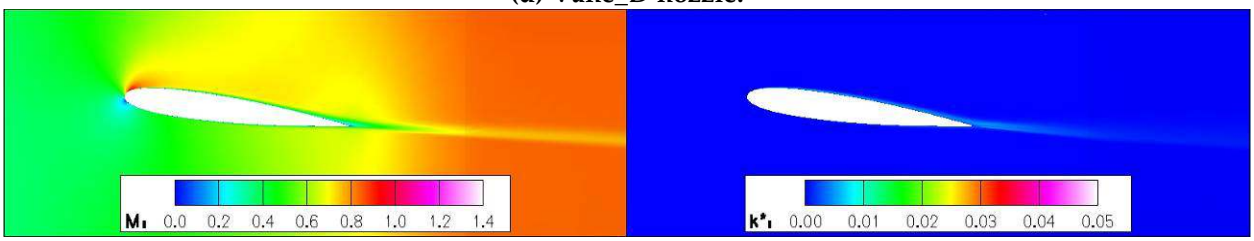

(e) Vane_E nozzle.

Figure 17: Mach number and turbulence contours at mid-span of lower vane for vane offset stream nozzles at take-off flow conditions.

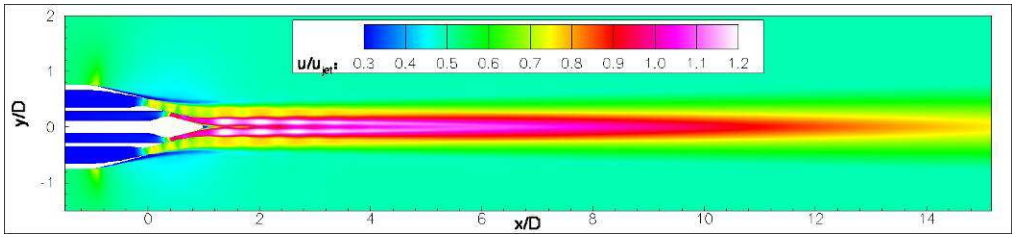

(a) 5BB baseline nozzle.

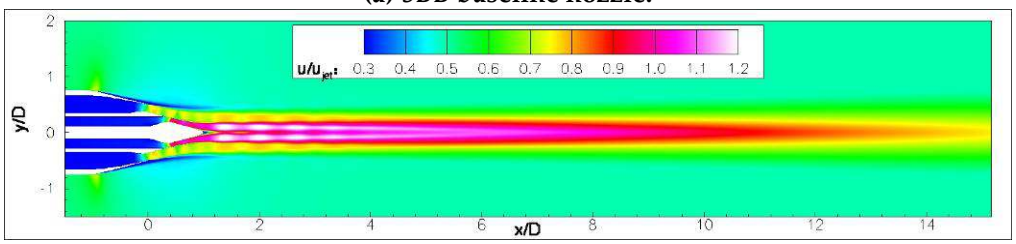

(b) Vane_cruise25 nozzle.

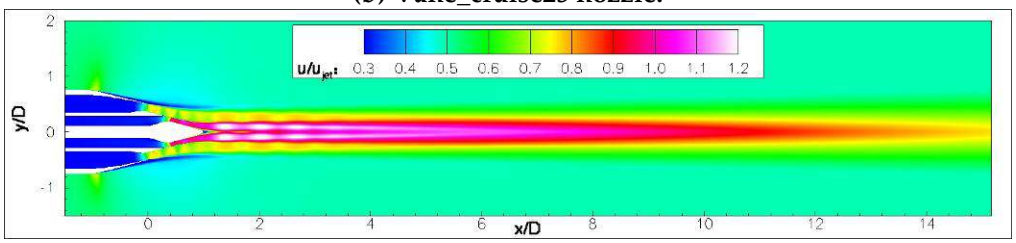

(c) Vane_cruise75 nozzle

Figure 18: Velocity contours on symmetry plane vane nozzles and baseline at cruise flow conditions

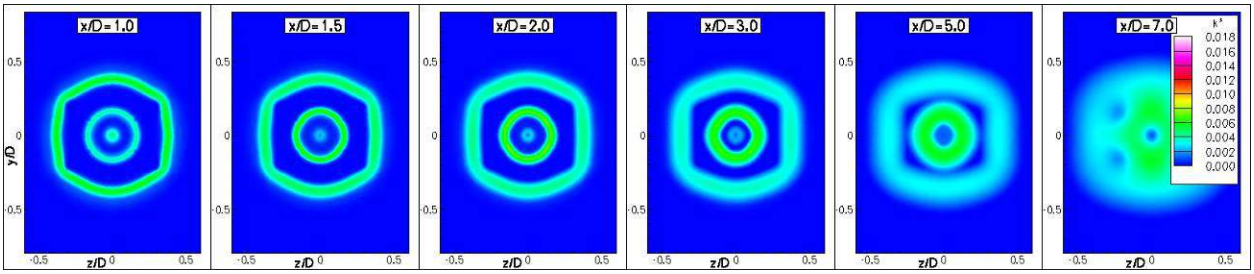

(a) Vane_cruise25 nozzle.

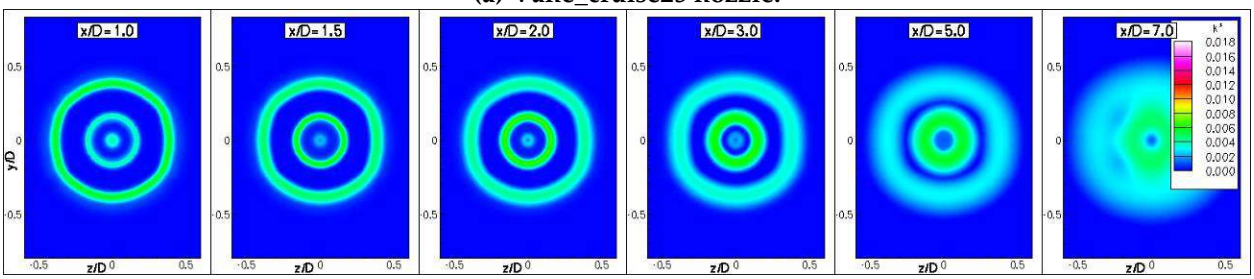

(b) Vane_cruise75 nozzle

Figure 19: Velocity contours at plume cross sections of vane offset stream nozzles at cruise flow conditions.

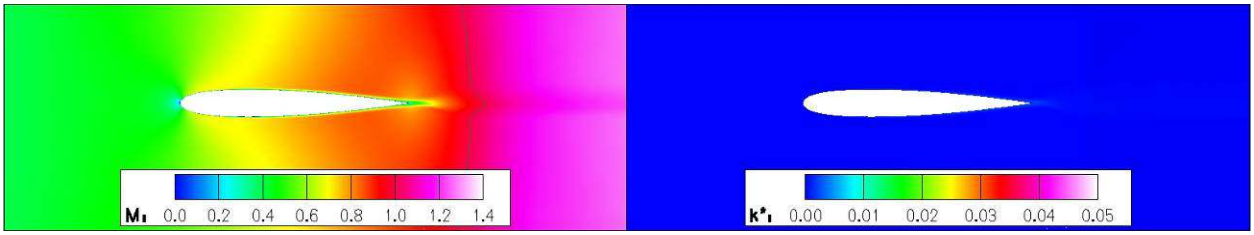

(a) Vane_cruise25 nozzle.

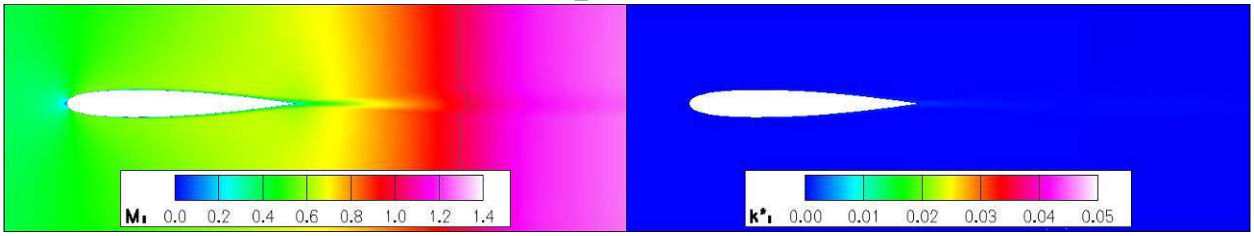

(b) Vane_cruise75 nozzle

Figure 20: Mach number and turbulence contours at mid-span of lower vane for vane offset stream nozzles at cruise flow conditions.

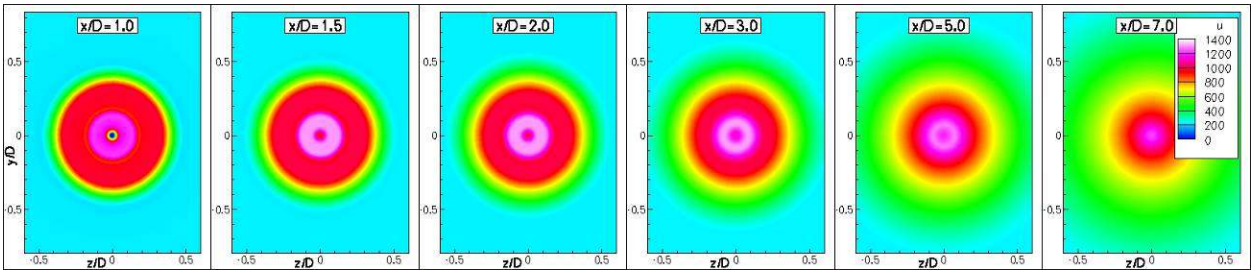

(a) CFD analyses data.

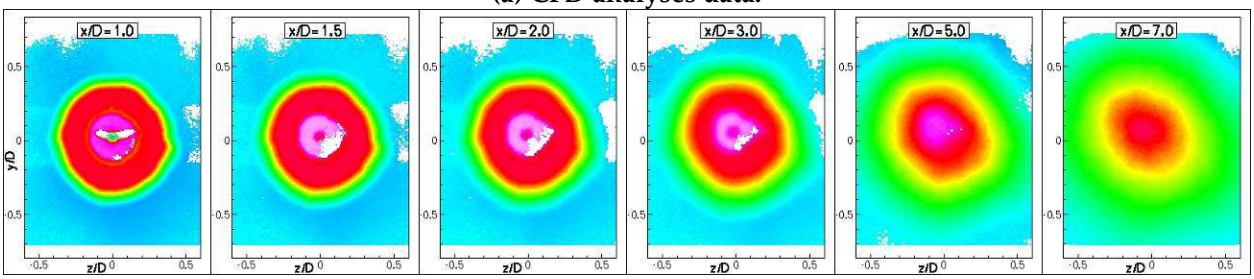

(b) Experimental PIV data.

Figure 21: Velocity contours of 5BB baseline nozzle at take-off flow conditions, M_∞=0.20.

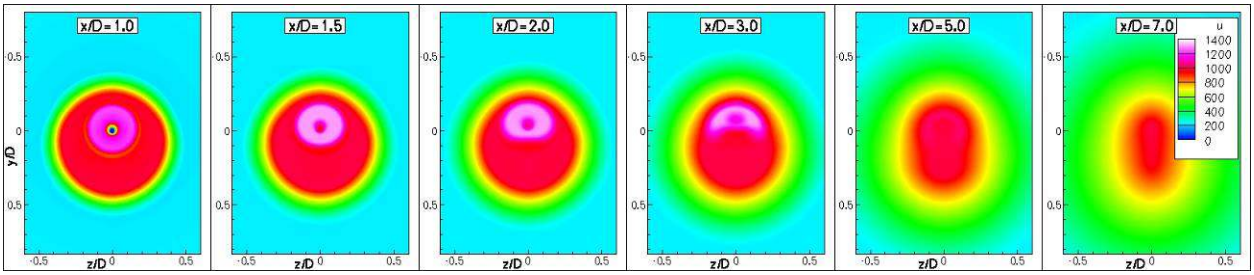

(a) CFD analyses data.

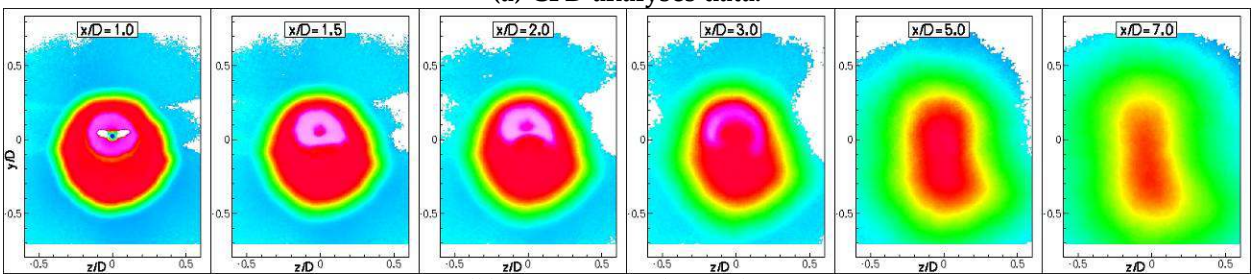

(b) Experimental PIV data.

Figure 22: Velocity contours of Sduct-5BB-45 offset stream nozzle at take-off flow conditions, M_∞=0.20.

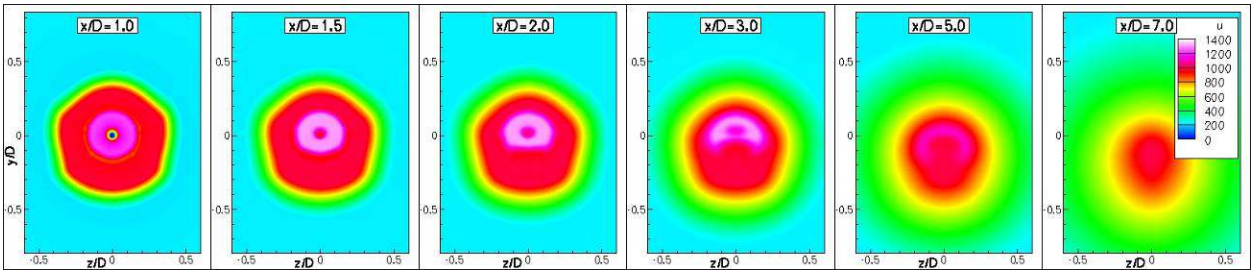

(a) CFD analyses data.

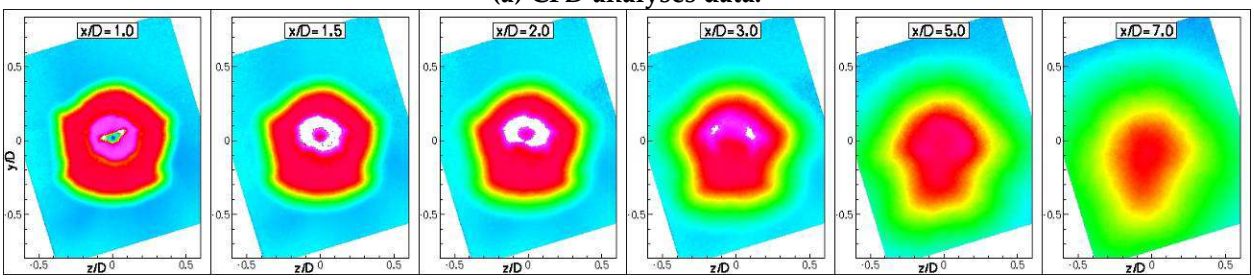

(b) Experimental PIV data.

Figure 23: Velocity contours of Vane_E offset stream nozzle at take-off flow conditions; M_∞=0.20.

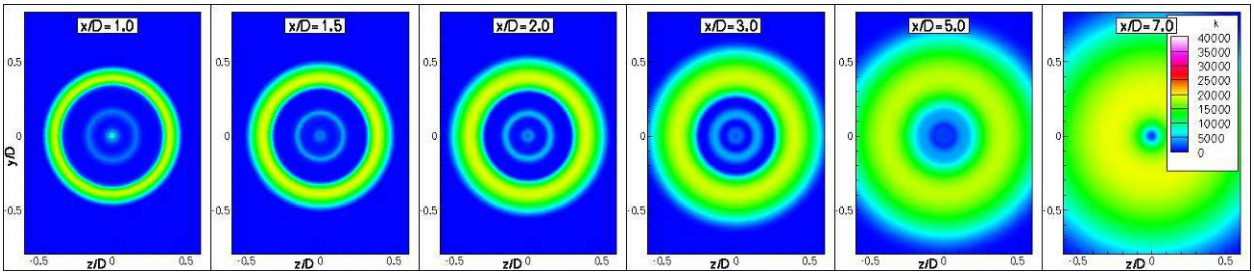

(a) CFD analyses data.

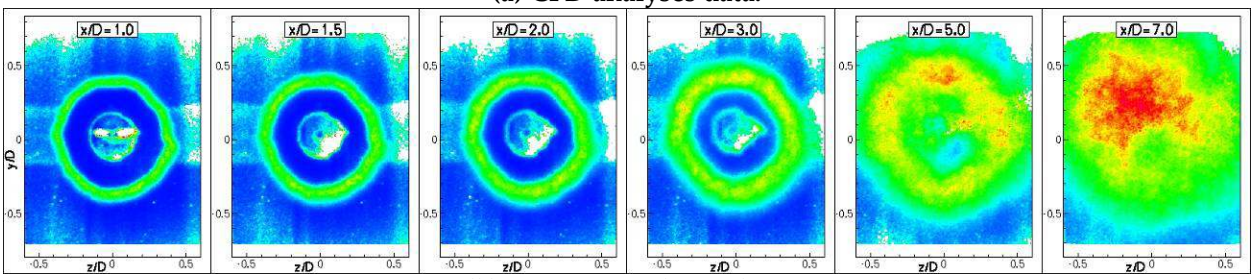

(b) Experimental PIV data.

Figure 24: Turbulence contours of 5BB baseline nozzle at take-off flow conditions, M_∞=0.20. k in units of ft²/s².

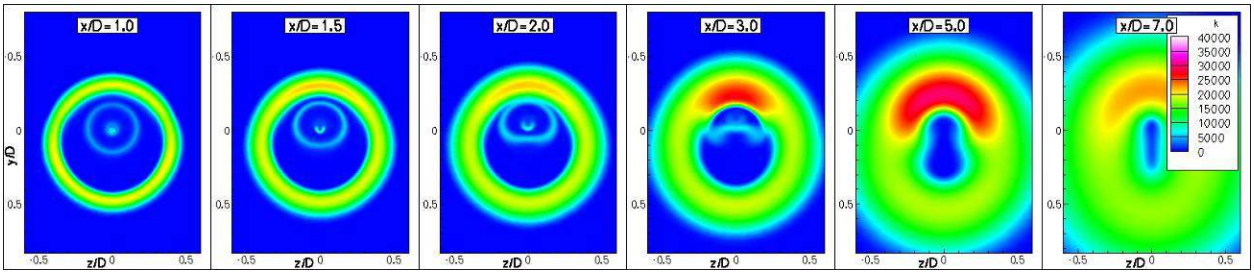

(a) CFD analyses data.

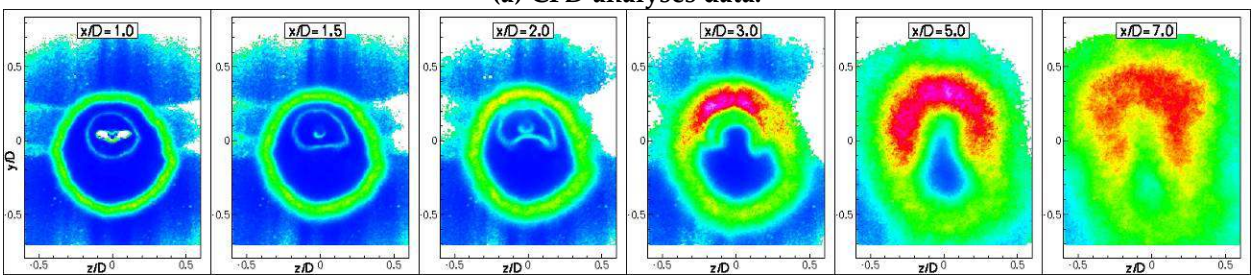

(b) Experimental PIV data.

Figure 25: Turbulence contours of Sduct-5BB-45 offset stream nozzle at take-off flow conditions, M_∞=0.20. k in units of ft²/s².

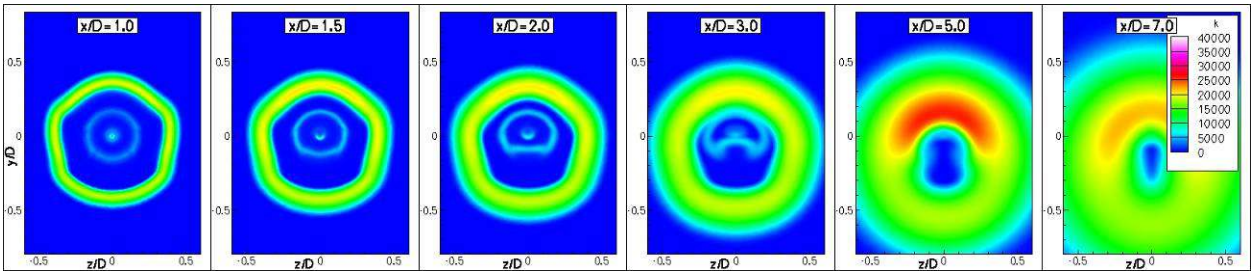

(a) CFD analyses data.

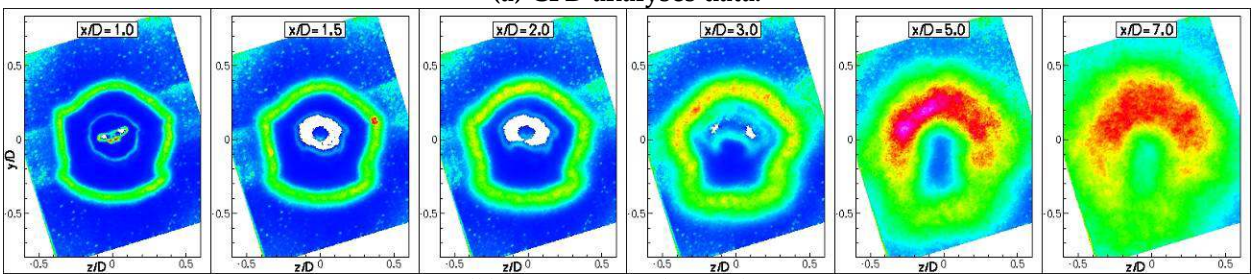

(b) Experimental PIV data.

Figure 26: Turbulence contours of Vane_E offset stream nozzle at take-off flow conditions; M_∞=0.20. k in units of ft²/s².